Introduction to Nanotechnology and Nanoscience – Class#19

Liwei Lin

Professor, Dept. of Mechanical Engineering
Co-Director, Berkeley Sensor and Actuator Center
The University of California, Berkeley, CA94720
e-mail: lwlin@me.berkeley.edu
http://www.me.berkeley.edu/~lwlin

Outline

- Paper 7 continue – Lab#2
- Conventional Electrospinning
- Nanofibers by Electrospinning (Paper #8)
- Small Project Presentations

Lab #2

University of California at Berkeley
College of Engineering
Mechanical Engineering Department

ME118/ME218N, Spring 2024 **Liwei Lin**

Lab #2
Due: One week after the last group's lab time

Lab 1 (Flexible Electronics)

We will continue using laser in lab #1 for the laser carbonization process and extending the process to the mechanical cutting scheme for Kirigami structures without using the conventional photolithography-based processes. A mechanical cutter is used to define complex resister patterns on designated material layers and/or cut through the layers by adjusting the applied force and speed. Please read through paper #7 carefully as lab #2 is based on the same process. TA will prepare the polymer samples and provide some guidelines for the operation of the mechanical cutter setup.

Final Project

- Don't copy ideas from others - you can state the differences of your idea and other paper(s) even if there is only one key difference while all other things are the same
- concept 10%, presentation 10%, written report 15%
- 4-page report, double columns like a research paper
- Title (name and affiliation), Abstract, Introduction, Design (concepts, principles, mechanisms), Fabrication, Analysis, Simulations (ME218N required), Discussions, Conclusion

Quiz I Results

ME 118

High : 79
low : 16
AVE : 53

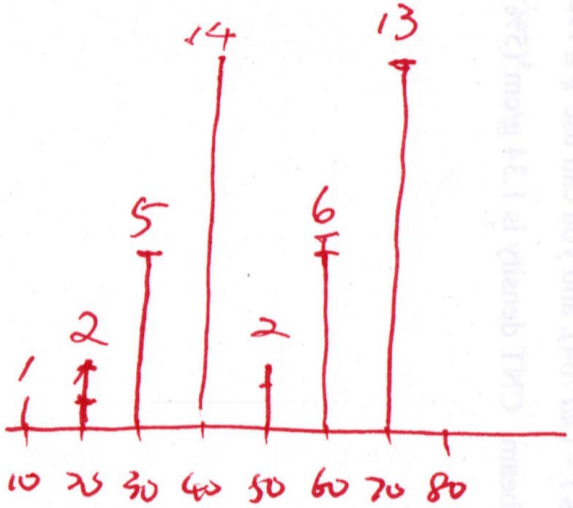

ME 218

High : 95
low : 36
AVE : 81

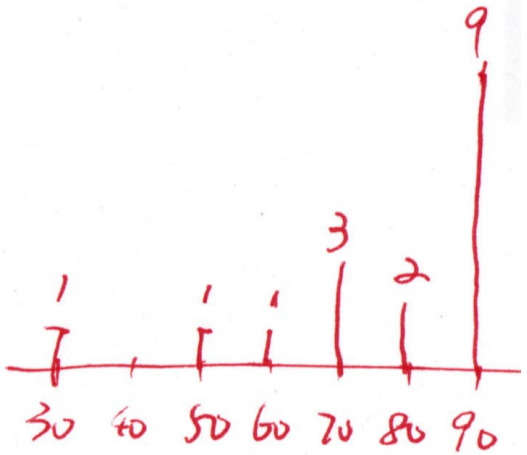

(a) Schematic illustration of the device:

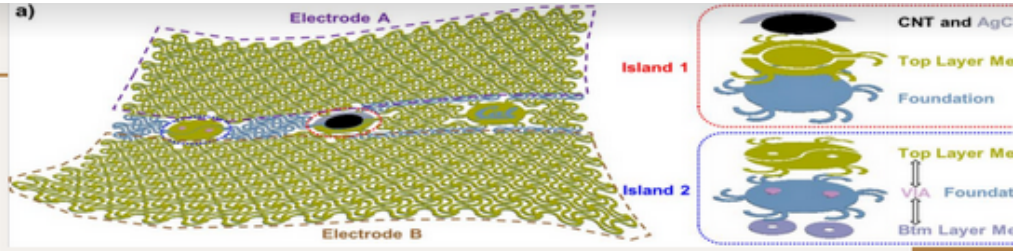

- Features stretchable electrodes A and B.
- The device features a flexible substrate with Electrodes A and B, indicating a stretchable electronic system capable of maintaining connectivity even when deformed or bent.
- Islands 1 and 2 are highlighted, suggesting localized functional areas with distinct components or materials on the substrate.
- Exploded views detail the layered structures of these islands, where Island 1 includes Carbon Nanotubes (CNT) and Silver Chloride (AgCl) on top of a top layer metal, pointing to specialized sensing or conductive functions.
- Island 2 displays a multi-layer configuration with a bottom metal layer, a foundational substrate, and a top metal layer, connected by VIAs, which are conductive through-holes that link the layers electrically.
- An additional, unmarked Island 3 is part of the network, presumably with its unique set of materials and function, contributing to the device's overall capabilities.

(b) Close-up optical image:

- The sensor consists of three electrodes: the working electrode the counter electrode, and the reference electrode, each serving a specific function in electrochemical measurements.
- The working electrode is where the electrochemical reactions of interest occur.
- The counter electrode serves as a surface to complete the electrical circuit by providing or receiving electrons.
- The reference electrode provides a stable reference potential against which the potential of the working electrode can be compared.
- The scale bar at the bottom right indicates the size of the features in the image, with 5 mm representing the length of the bar, helping to understand the actual size of the components.
- Surrounding stretchable filaments visible.

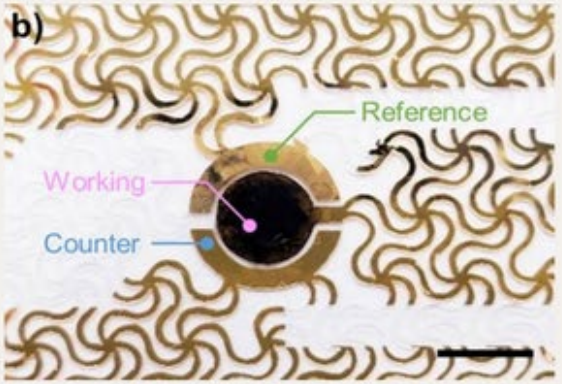

- Scale bar: 5 mm.

(c) SEM image:

- Depicts the CNT working electrode.

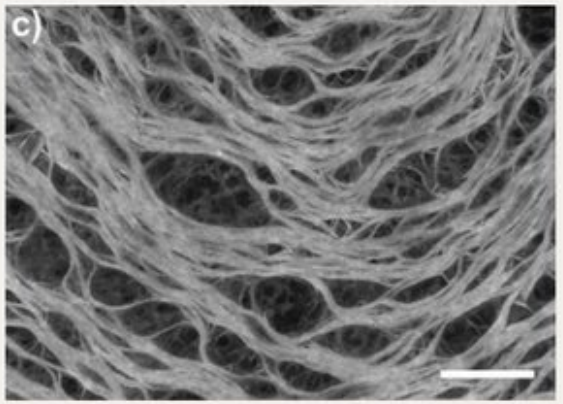

- Scale bar: 5 μm.

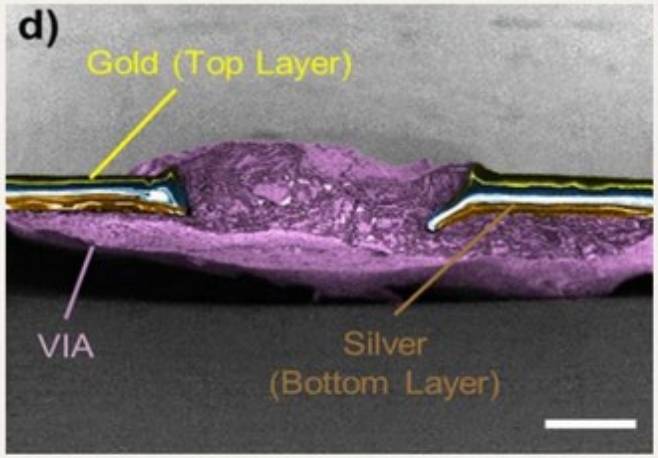

Scale bar: 100 μm.

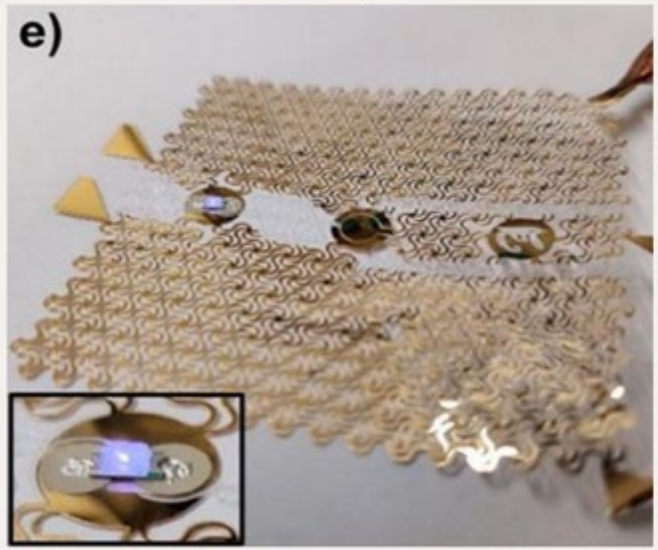

(d) False-colored SEM image:

- "Gold (Top Layer)" is marked in yellow, indicating the uppermost conductive layer in the VIA structure, which is made of gold.
- "Silver (Bottom Layer)" is marked in orange, designating the lower conductive layer, which is made of silver.
- The VIA itself is indicated with a white label, demonstrating the pathway that electrically connects the top layer and bottom layer.
- This VIA is essential for the multi-layer circuit's functionality, allowing for complex circuits to be built in compact spaces.

(e) Optical image demonstrating:

- A stretchable substrate with conductive, wavy filaments and several distinct islands with electronic components, including an LED.
- There are triangular points of contact at the corners, likely providing stable connection points or facilitating the integration with other systems.
- The wavy pattern of the filaments allows for stretching & bending while staying electrical connectivity, essential for various applications requiring flexibility.

(f–h) Illustrative diagrams showing the working scenarios of:

- The diagrams (f)-(h) depict the functions of a multi-layered wearable device with applications in biometric monitoring and drug delivery:
- Diagram (f) represents a cross-section of the device with a top layer containing Electrode A and Electrode B, connected through VIAs (Vertical Interconnect Access) to the bottom layer with corresponding Pad A and Pad B. This setup is typically used to power an LED, suggesting the device can provide visual feedback or signaling.
- Diagram (g) illustrates the device configured for sweat extraction with a hydrogel substance placed between two electrodes. When voltage is applied, the hydrogel can encourage sweat to be extracted from the skin for analysis or drug delivery purposes.
- Diagram (h) details the sweat sensing function of the device, where it utilizes a three-electrode system: a reference electrode, a counter electrode, and a working electrode submerged in sweat. The potential difference measured across these electrodes can give information about the chemical composition of the sweat, useful for health and performance monitoring.

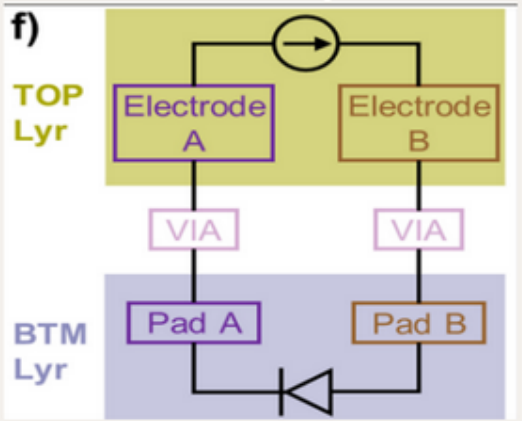

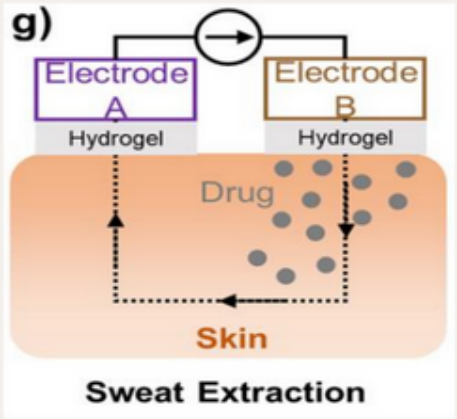

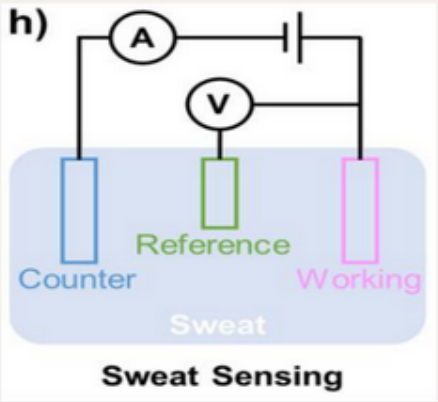

- Conducted on four representative "dummy sweat" solutions.
- Image (i) shows linear scanning voltammetry curves for four different concentrations of a "dummy sweat" solution, with each curve representing a different concentration of uric acid (UA) and tyrosine (Tyr), simulating the chemical makeup of human sweat.
- Image (j) is a bar graph comparing the current density achieved when sensing uric acid with four different electrode materials: carbon nanotubes (CNT), gold, glassy carbon, and printed carbon. CNT shows the highest current density, indicating its superior sensitivity or conductivity for this application.
- Image (k) provides an optical image of the actual device, highlighting its mechanical flexibility. The image shows the device being deformed by a stirring rod, which demonstrates the device's durability and its potential application in wearable technology where flexibility and durability are crucial.

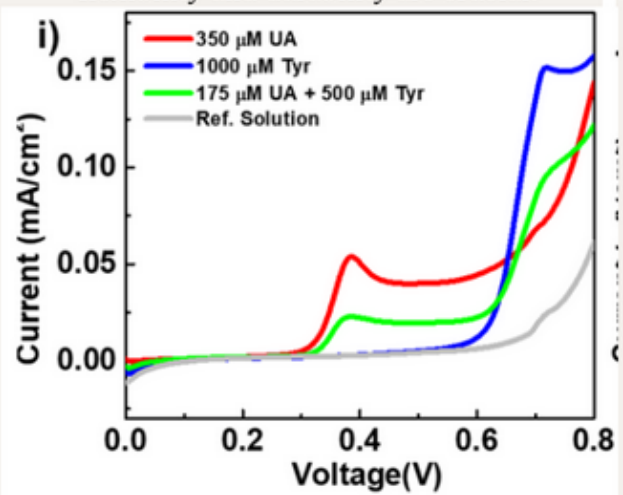

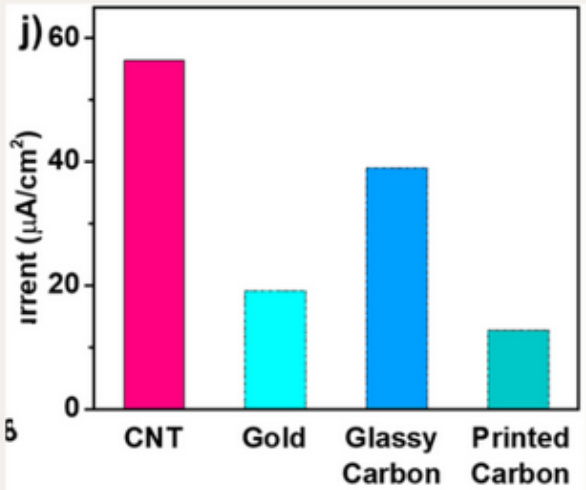

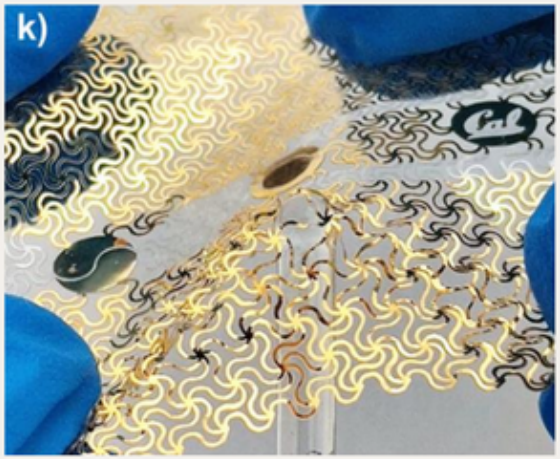

Respiratory Sensory Advantages of MultiLayer Electronics.

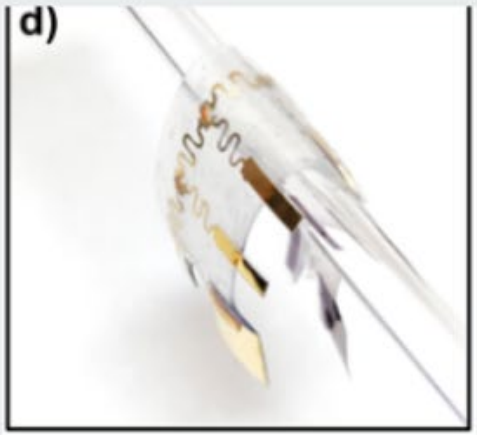

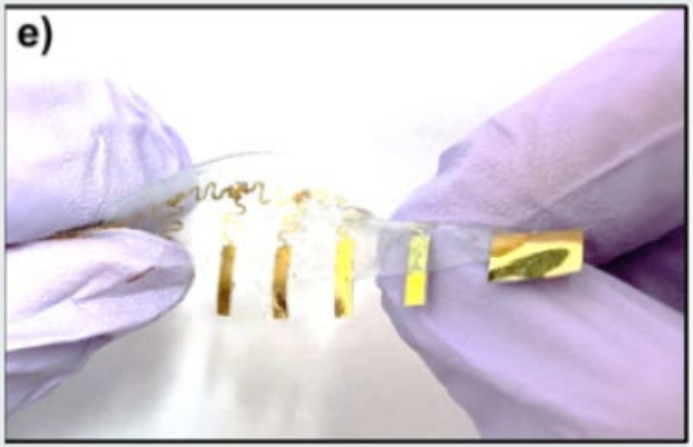

Main Characteristics

- Works with five surface mount temperature sensors. (NA of 1.3mm^2)
  - Made out of TFPT0603. Alumina substrate with nickel PTC thin Film element
  - Resistance value of 100-1k Ohm +- 0.5 % (operable from -55 to +70-[1
- Monitor respiration patterns without being obstructive is key for HCI
- Conditions for heat transfer and resistivity calculations are still on work

- Exposing the sensors' top, they can provide temperature readings.
- Used two sensors to average out temperature gradient.
- Distance of 7.5mm

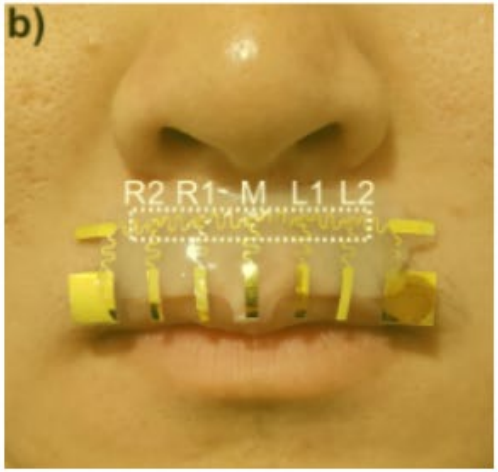

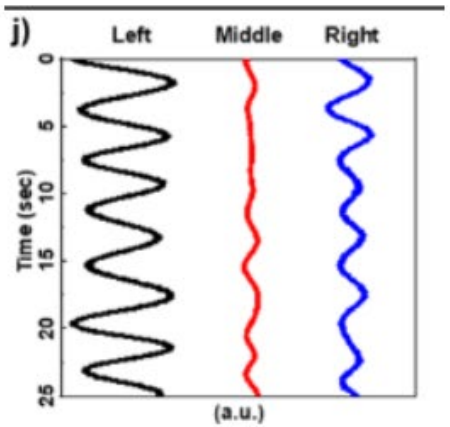

Complications for Temp Calculations

- Bulk properties of fluids heat transfer are known, but nanoscale sensor theory fails in some circumstances. [4]
- Size is so small that natural convection becomes insignificant. (Control Volume is so small that differences in density become non-existing.
- Guo et al. [13] investigated the size effect on heat transfer in microdevices. These studies suggest that larger surface area to volume ratio in the heated solid will have an impact on heat transfer coefficient.

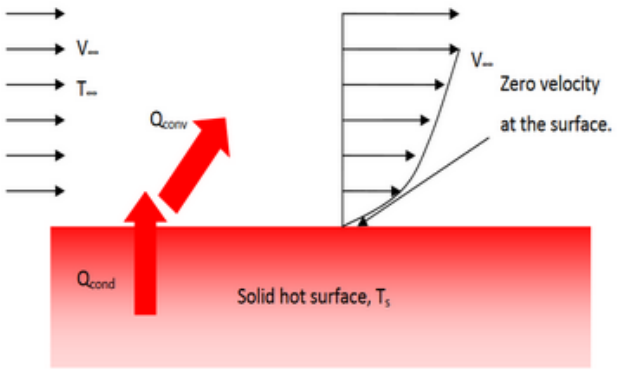

Fig. 1: Forced convection.

Calibration Issues for Temperature

- Grashof number estimated on mentioned paper for a silicon beam as flat plate of 20 micrometer to be on the order of 10^-5 [4]
- Bulk properties for h for free convection are usually 10-25 W/m^2K
- Scaling for vertical or horizontal plate equations (Rayleigh → Nu -and Pr if feeling fancy-) would suggest an h value of 100 Wm^2K (let Peirs et al. [6])
- This would suggest error calculations

$$\overline{\mathrm{Nu}} = \frac{\frac{1}{L}\int_0^L h_x \, dx \, L}{k} = \frac{\overline{h}L}{k}$$

$$\mathrm{Gr}_L = \frac{g\beta(T_s - T_\infty)L^3}{\nu^2}$$ for vertical flat plates

$$\overline{\mathrm{Nu}_L} = 0.069\,\mathrm{Ra}_L^{1/3} Pr^{0.074} \qquad 3 * 10^5 \leq \mathrm{Ra}_L \leq 7 * 10^9$$

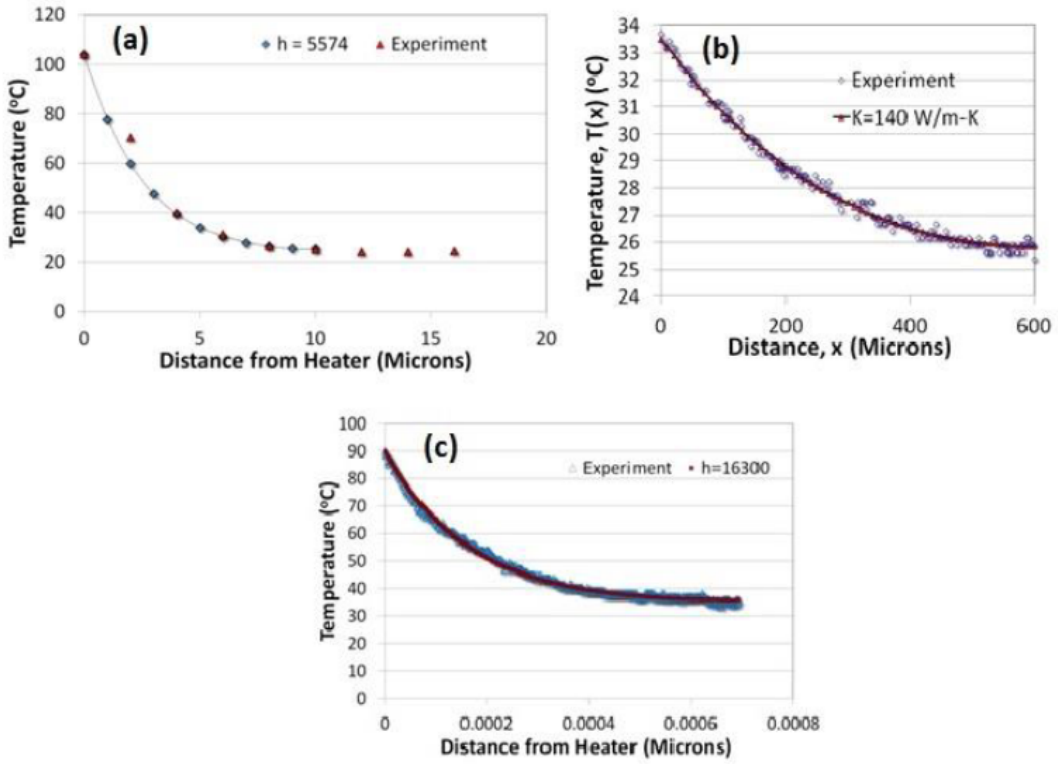

Figure 2.6 Validation of the proposed empirical relation given in equation 2.16 for three different cases, (a) 5 μm wide and 50 nm thick freestanding silicon nitride, (b) 10 μm wide and 20 μm thick silicon specimen with no floor and (c) 10 μm wide and 20 μm thick silicon specimen with a neighboring surface at 2 μm distance

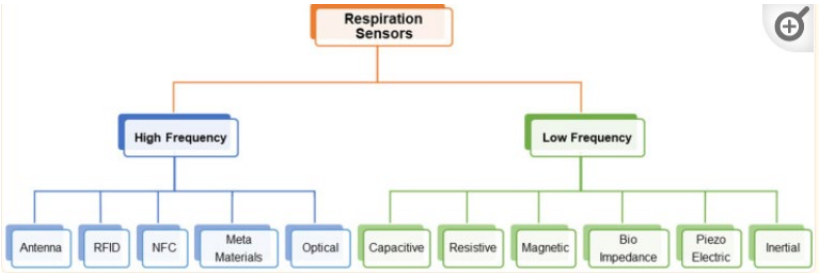

Compared to Other Technologies

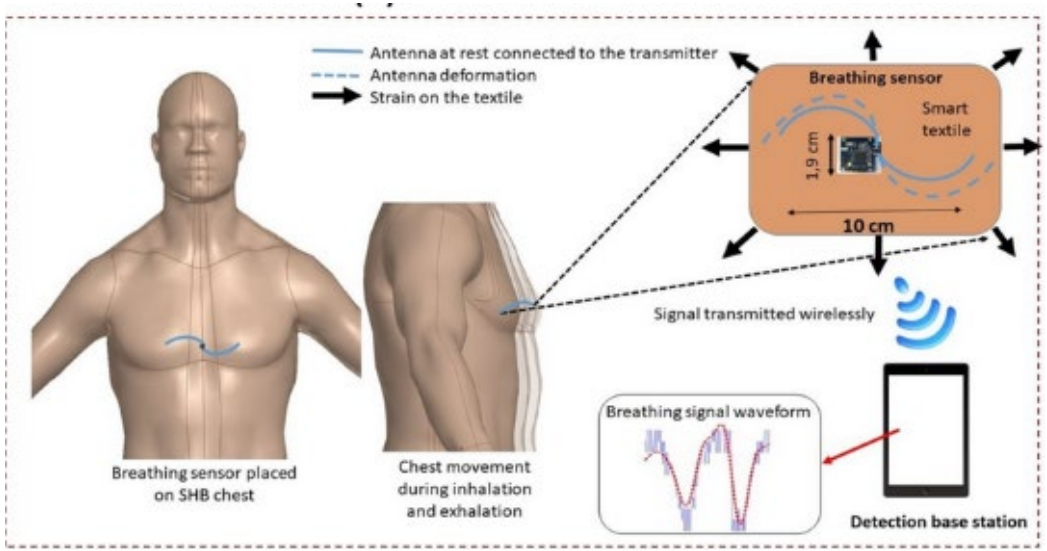

- Can measure deformation and temperature!
- Similar sensitivity devices are way bigger and required more equipment [2][3]
- RSSI using AMS SL900A with power sensitivities of −6.9 dBmW and −15 dBmW
- -40 to 150C range of Temperature

Sources

[1] https://www.vishay.com/docs/33017/tfpt.pdf

[2] https://www.mdpi.com/1424-8220/23/17/7518

[3] https://www.ncbi.nlm.nih.gov/pmc/articles/PMC10490703/

[4] https://etda.libraries.psu.edu/files/final_submissions/11142

Fabrication of Stretchable Mesh

Start with a mylar film layer with PET adhesive on both sides.

Tunnel cut both sides and deposit metal on both sides to create metallization layers.

Evaporate gold and remove the adhesive on the top side, and screen print silver on the bottom and cure at 110 C.

A “through cut” creates the mesh structure, and fill the holes with silver epoxy then cure to create VIAs.

Lastly, deposit AgCl and CNTs to form the final electrode.

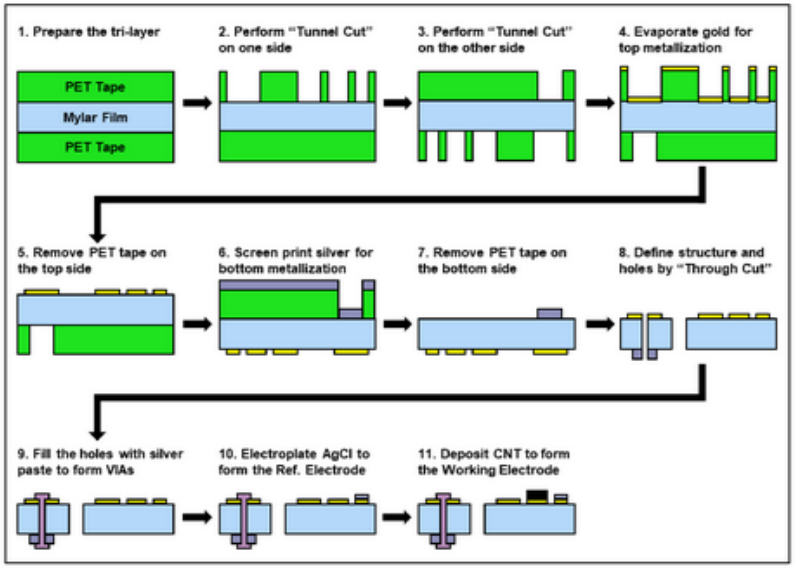

Figure S8

Facile Fabrication of Multilayer Stretchable Electronics via a Two-mode Mechanical Cutting Process, Renxiao Xu, Peisheng He, Guangchen Lan, Kamyar Behrouzi, Yande Peng, Dongkai Wang, Tao Jiang, Ashley Lee, Yu Long, and Liwei Lin

Application of Stretchable Smart Mesh

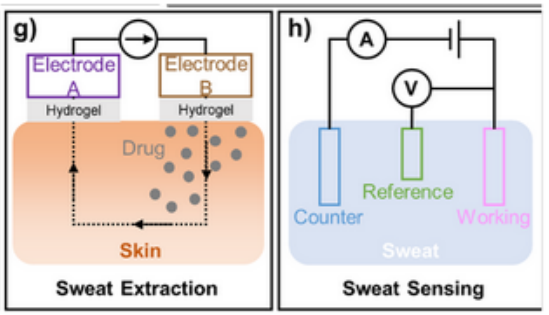

The mesh has apparent applications in biomedicine.

Sweat extraction and analysis is useful in detecting diseases, like cystic fibrosis, and can be used to measure glucose levels in relationship to sweat composition.

Sweat inducing drugs can be attached to thoroughly cover all electrodes so that chemicals of interest can be oxidized and measured.

On the right is an LSV test, the peaks in current correlate to concentration of chemical.

Sensitivity is calculated by fitting the peak slopes to concentration graphs.

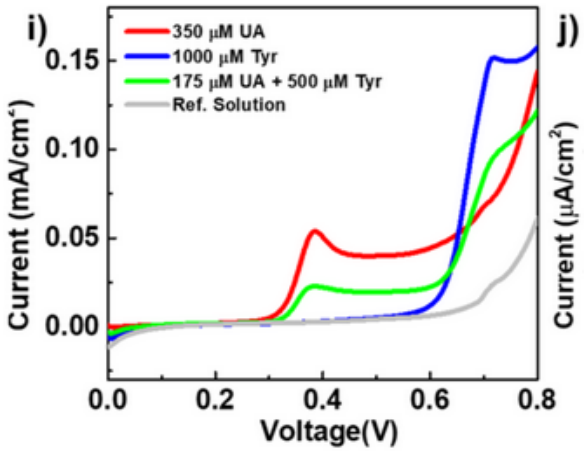

Figure 5H, 5G, 5I

Facile Fabrication of Multilayer Stretchable Electronics via a Two-mode Mechanical Cutting Process, Renxiao Xu, Peisheng He, Guangchen Lan, Kamyar Behrouzi, Yande Peng, Dongkai Wang, Tao Jiang, Ashley Lee, Yu Long, and Liwei Lin

Emaminejad, S.; Gao, W.; Wu, E.; Davies, Z.A.; Yin Yin Nyein, H.; Challa, S.; Ryan, S.P.; Fahad, H.M.; Chen, K.; Shahpar, Z.; et al. Autonomous sweat extraction and analysis applied to cystic fibrosis and glucose monitoring using a fully integrated wearable platform. Proc. Natl. Acad. Sci. USA **2017**

Usage of CNTs

CNT properties are what allow these devices to operate as chemical sensors due to their high electrical conductivity and surface area (related to its sensitivity).

"For a 0.35 mM UA solution, a device with CNT as the working electrode can yield a peak height of 56.5 μA/cm2, evidently higher than commonly used electrode materials, such as gold (19.1 μA/cm2), glassy carbon (38.9 μA/cm2), and printed carbon (12.7 μA/cm 2)."

CNTs are also chemically resistant and biocompatible, and further applications of nanoscale materials, like quantum dots and graphene, are being investigated for use in biosensors.

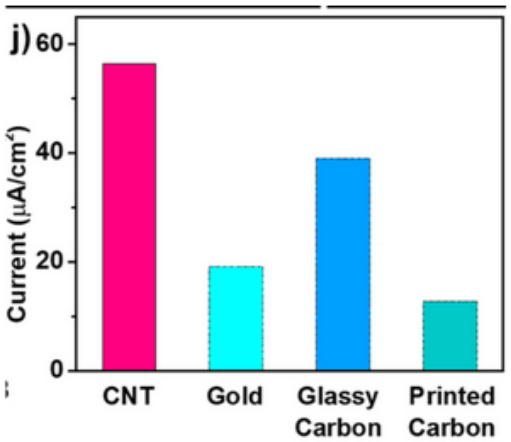

Figure 5J

Facile Fabrication of Multilayer Stretchable Electronics via a Two-mode Mechanical Cutting Process, Renxiao Xu, Peisheng He, Guangchen Lan, Kamyar Behrouzi, Yande Peng, Dongkai Wang, Tao Jiang, Ashley Lee, Yu Long, and Liwei Lin

Ehtesabi H, Kalji SO. Carbon nanomaterials for sweat-based sensors: a review. Mikrochim Acta. 2024 Jan 5;191(1):77. doi: 10.1007/s00604-023-06162-7. PMID: 38177621.

Material Properties

The mechanical properties of the mesh make them good for on-skin usage, able to stretch beyond skin capabilities and resist localized pressure due to fabrication quality and structure.

The right figure shows a uniaxial tension test, where a J-shaped response (top) is desired (most biological materials behave this way). It holds well in twisting, bending, and buckling.

The electrical performance holds under 30% elongation with no more than a 10% change in resistance. The steep part of the curve shows when the filaments straighten and strain is resisted.

The mesh can withstand 85% X tension and 103% Y tension before the first fracture, but load redistribution lets it withstand more strain before another failure while still maintaining structural integrity and performance.

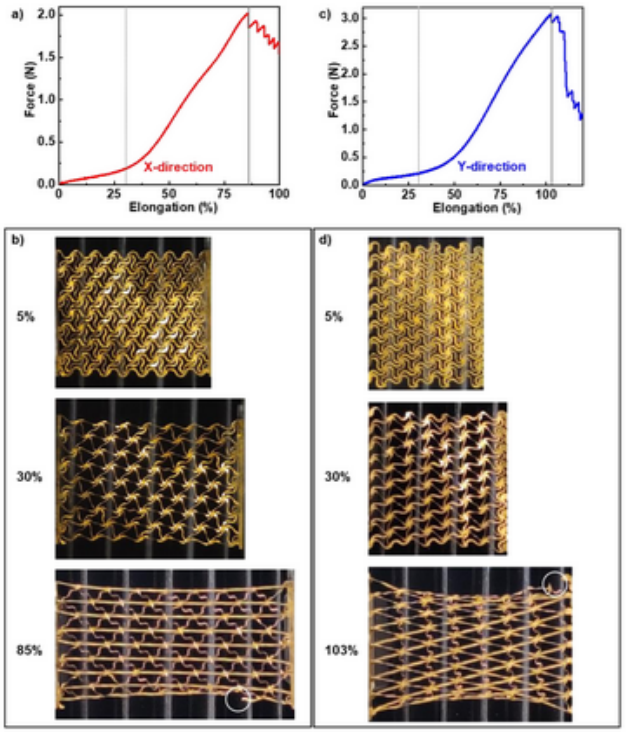

Figure S10

Facile Fabrication of Multilayer Stretchable Electronics via a Two-mode Mechanical Cutting Process, Renxiao Xu, Peisheng He, Guangchen Lan, Kamyar Behrouzi, Yande Peng, Dongkai Wang, Tao Jiang, Ashley Lee, Yu Long, and Liwei Lin

Using Accessible Components

The two-mode cutting process allows for integration of commercial electrical components.

The below diagram shows 5 commercial temperature sensors connected in series on mylar film with gold interconnects.

Applied below the nose, most of the circuitry is protected by the elastomeric encapsulations, with only the sensors exposed. These sensors detect the temperature change caused by inhalation and exhalation and capture both nostrils. Figure 6C shows how the interconnects allow for ductility.

Facile Fabrication of Multilayer Stretchable Electronics via a Two-mode Mechanical Cutting Process, Renxiao Xu, Peisheng He, Guangchen Lan, Kamyar Behrouzi, Yande Peng, Dongkai Wang, Tao Jiang, Ashley Lee, Yu Long, and Liwei Lin

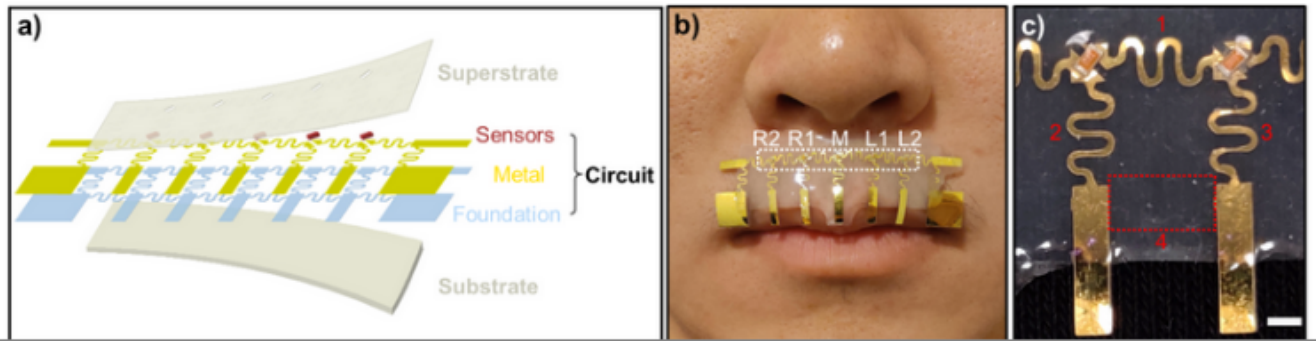

Figure 6A, 6B, 6C

Summary

- This section of the paper details a specific aspect of a stretchable, skin-mounted module designed for monitoring human breathing patterns
- focuses on the mechanical design and electrical architecture of the module, fabrication process, and its application in monitoring and analyzing breathing patterns, including its utility in diagnosing and managing respiratory-related conditions.

Mechanical and Electrical Design

- Four serpentine-shaped interconnects (one unit)
- Interconnect 1: electrical trace joining sensors in series
- Interconnect 2 & 3: terminals for potential measurement
- Interconnect 4 (Mylar film): wire without conductors for balancing mechanical loads + providing deformability
- Overall softness and deformability due to low modulus elastomeric encapsulations, thinness, and serpentine design (stretch, twisted and wrapped)

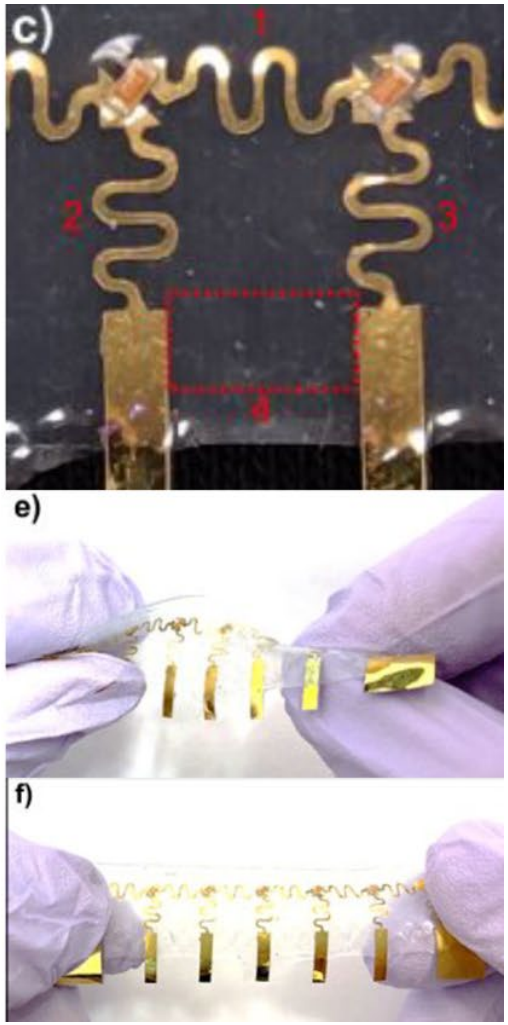

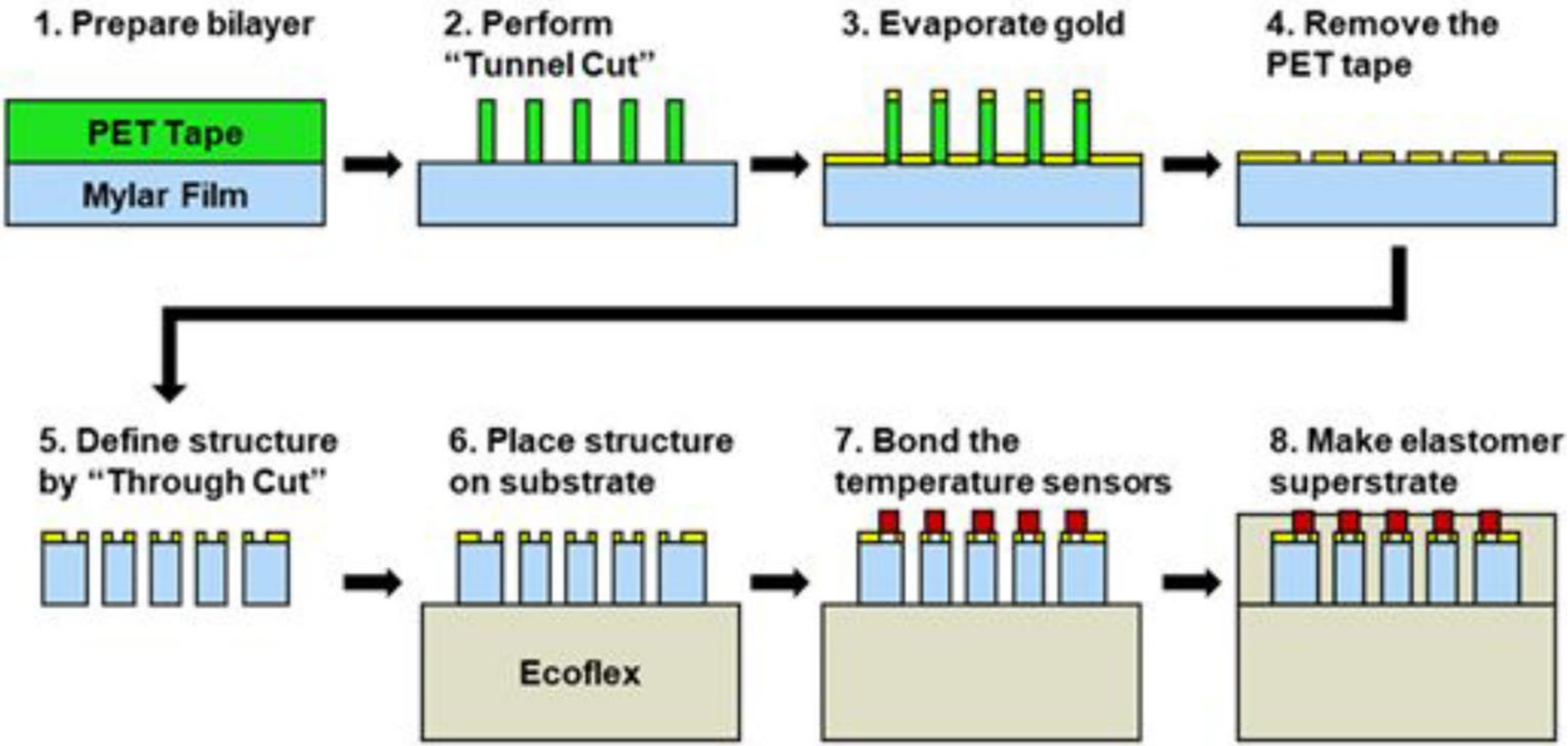
1. Prepare bilayer
PET Tape
Mylar Film
2. Perform "Tunnel Cut"
3. Evaporate gold
4. Remove the PET tape
5. Define structure by "Through Cut"
6. Place structure on substrate
Ecoflex
7. Bond the temperature sensors
8. Make elastomer superstrate

Application in Monitoring Breathing Patterns

- device can aid in diagnosing respiratory conditions th
  - Examples include asthma, sleep apnea, and covid-19 symptoms
- Able to distinguish between normal breathing, nasal congestion, and deep breathing through temperature changes seen by sensor

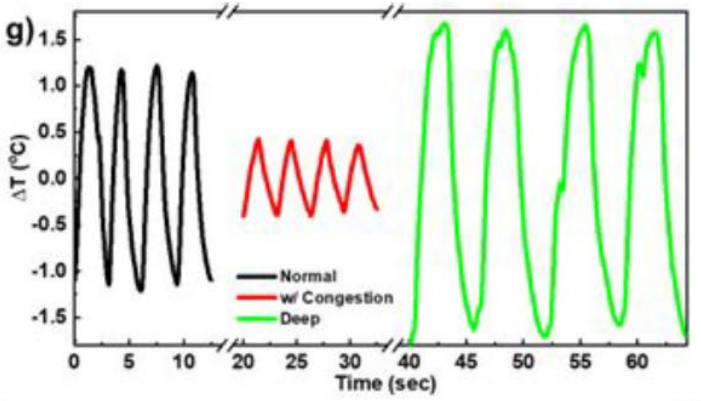

Breathing patterns from right nostril of healthy male

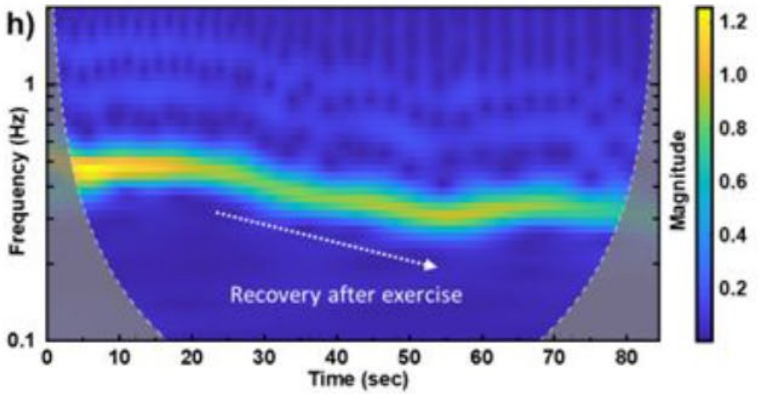

Breathing patterns from same volunteer after mild exercise

Application in Monitoring Breathing Patterns (Cont.)

- Furthermore by connecting the five sensors in series and reading signals from each sensor can evaluate symmetry in breathing patterns
  - Septum deviation, common cold, sinusitis, and nasal plyposis
- Signals from sensors placed near each nostril (L1, L2, R1, R2, and M)
- Potential for mapping airflow velocity, estimating thoracic pressure, and identifying sleep related breathing

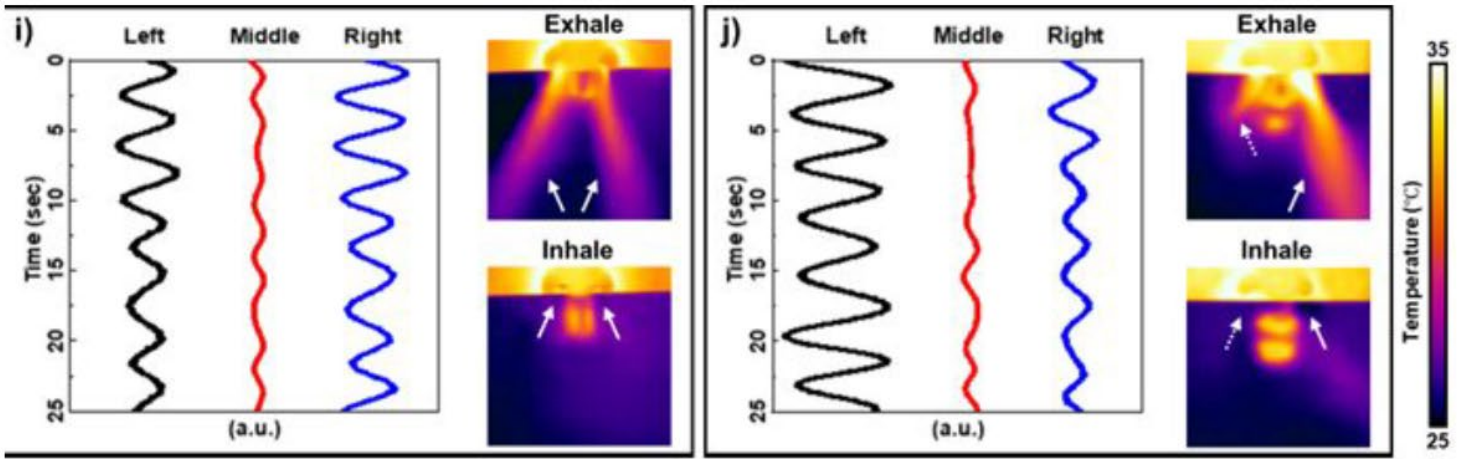

Electrochemical Testing of WSSC

Tested via CV, GCD, and EIS tests

CV, potential window was chosen 0.8V for one unit and 2.4V for the entire device

GCD, calculated capacitance C_A

EIS, recorded real and imaginary parts of impedance(Z and Z´)

- Cyclic Voltammetry
- Galvanostatic Charge-Discharge
- Electrochemical Impedance Spectroscopy
- $C_A = I\triangle t/\triangle VA$
  - I = discharge Current
  - $\triangle t$ = discharge time
  - A = nominal area of electrode
  - $\triangle V$= potential window

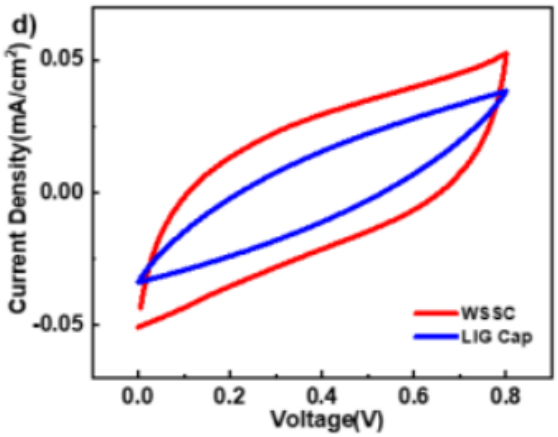

Deposition of AgCl and CNT

1. Plating silver at Pt plate
2. After deposition of silver ,AgCL was electrodeposited with NaCl solution.
3. The CNT was then deposited by drop-casting a CNT dispersion on the gold current collector and dried for 2 min.
4. This process was repeated about 5 times until CNT covered the electrode area.
5. Surfactants were washed away with DI water

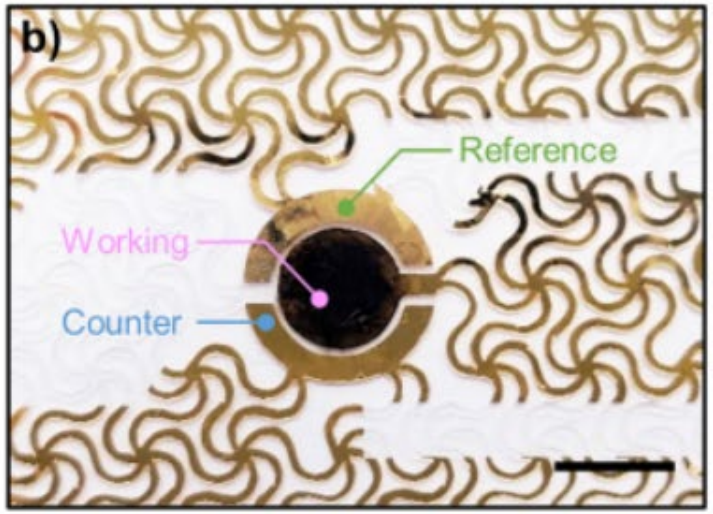

Testing of Breathing Monitoring Module

1. Single sensor, Gamry Reference 600
2. 5 sensors in series, USB-6341
3. Precise current source, Keithley 6220

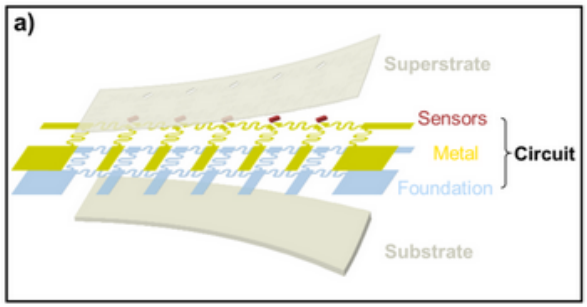

- Illustration of Breathing Monitoring Module
- National Instruments USB6341
- Reference 600 Gamry
- Keithley 6220

https://www.researchgate.net/figure/National-Instruments-NI-USB-type-6341-data-acquisition-system-14_fig3_296333484
https://www.gamry.com/support-2/legacy-devices/reference-600-legacy/

https://www.axiomtest.com/Power-Supplies/DC-Power-Supplies,-Low-Voltage-%28less-than-60V%29,-Low-Current-%28less-than-60A%29/Keithley/6220/DC-Precision-Current-Source/

Berkeley UNIVERSITY OF CALIFORNIA

Finite Element Analyses of Deformation

- Three dimensional FEA simulation by ABAQUS
- Aimed to predict deformed geometric details and reversible stretchability values.
- Modeled with quadrilateral shell elements (S4R) and used “Composite Layup” function for different regions in the device.
- The most complex region was defined by 5 layers
- Measured reversible stretchability by testing overall elongation,

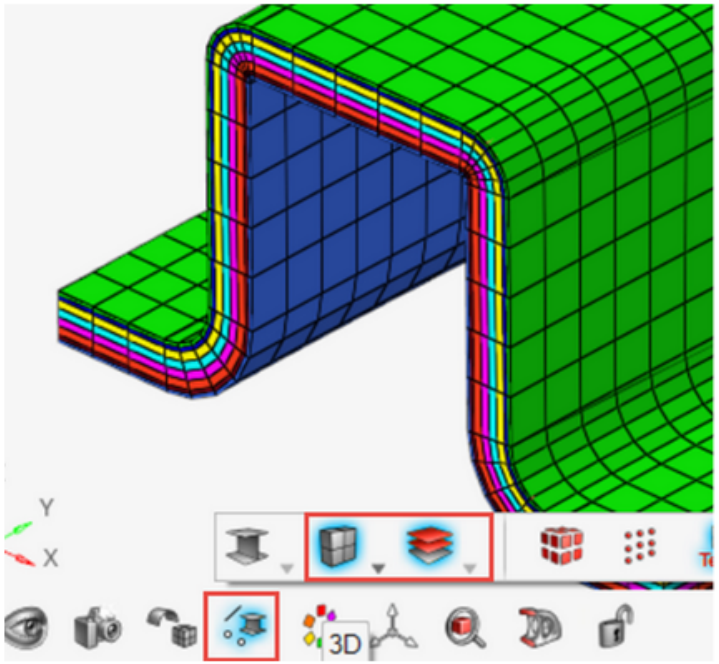

Reference Image of FEA

https://2021.help.altair.com/2021/hwdesktop/hm/topics/pre_processing/composites/tutorial_composite_analysis_c.htm

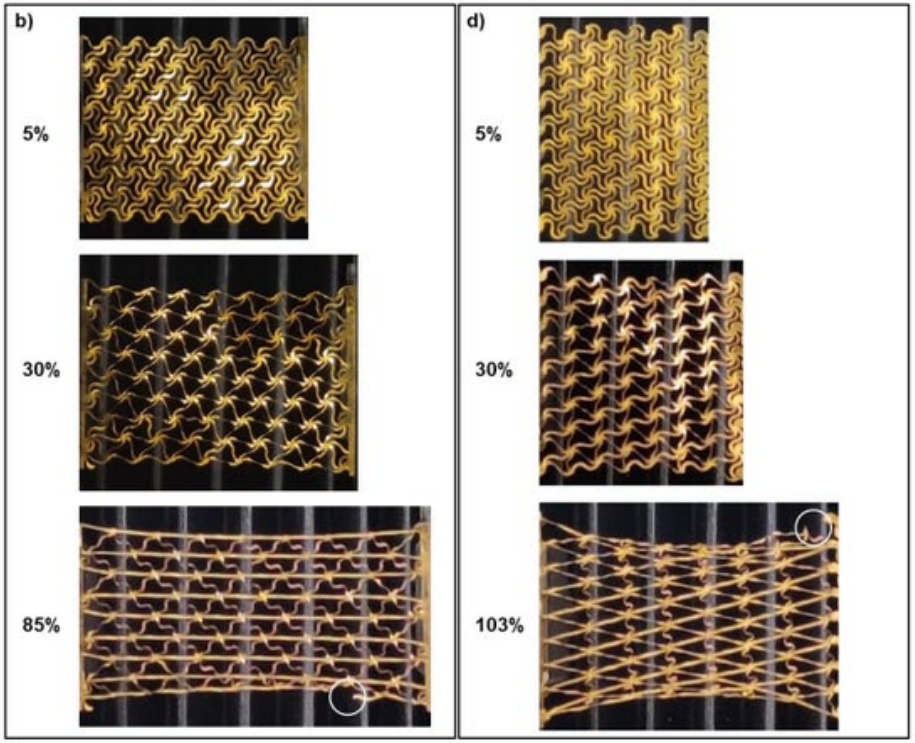

Material	Thickness	Young's Modulus	Poisson's Ratio	Elastic Limit
PET	25 μm	4 GPa	0.4	
Adhesive	15 μm	20 MPa	0.475	
PVA Electrolyte + LIG	10 μm	20 MPa	0.475	
Gold	100 nm	78 GPa	0.44	0.3%
Mylar	40 μm	4GPa	0.4	

5 layers, from top to bottom

Introduction to Nanofibers

- The smallest polymer fiber contains one polymer molecule, typically having a diameter of a few tenths of a nanometer.
- Oligomers of polyethylene have been observed in single-layer crystal-like arrays with a diameter of around 0.4 nm.

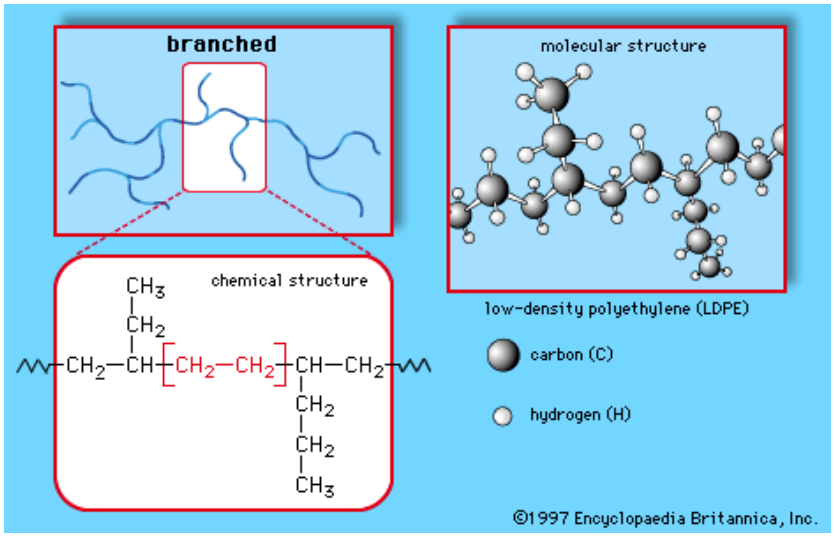

Introduction to Nanofibers: DNA

- The DNA double helix comprises two backbone chains with a diameter of approximately 2.5 nm
- Observation of DNA molecules in solution reveals fiber-like properties such as extension and transport in response to external forces
- Collagen molecules twist around each other to form triple helix fibers, which play a crucial role in higher levels of organization, such as tendon formation

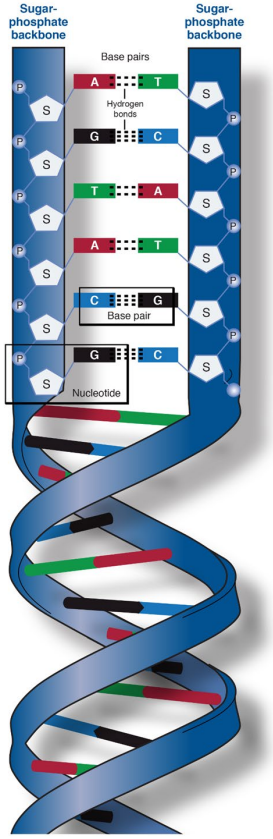

Introduction to Nanofibers: Commercial Processes

- Expansion of foam until most of the polymer converts to fibers, yielding fibers around 100 nm in diameter.
- Particles of polytetrafluoroethylene from dispersion polymerization processes adhere to each other, forming small fibers when pulled apart.
- Gentle scratching of molded polytetrafluoroethylene with coarse sandpaper generates many fibers with nanoscale diameters on the surface.

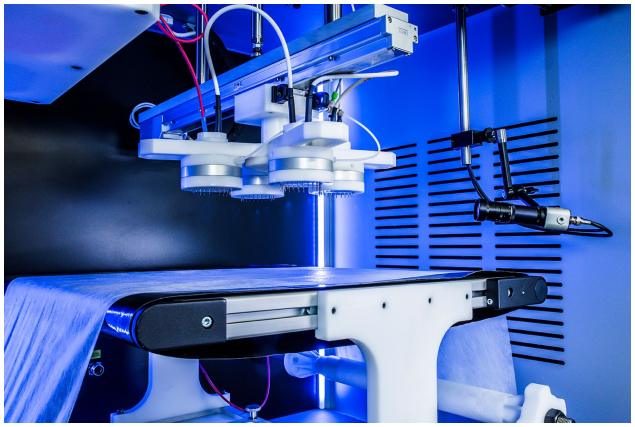

Introduction to Electrospinning

- A liquid polymer is held in the solution reservoir and flows at a constant rate
- In the emitter, charges accumulate at the surface of the liquid.
- The fluid will begin to emit when electrostatic repulsion is larger than the surface tension.
- When charges leave the liquid, the polymer will solidify on the collector.

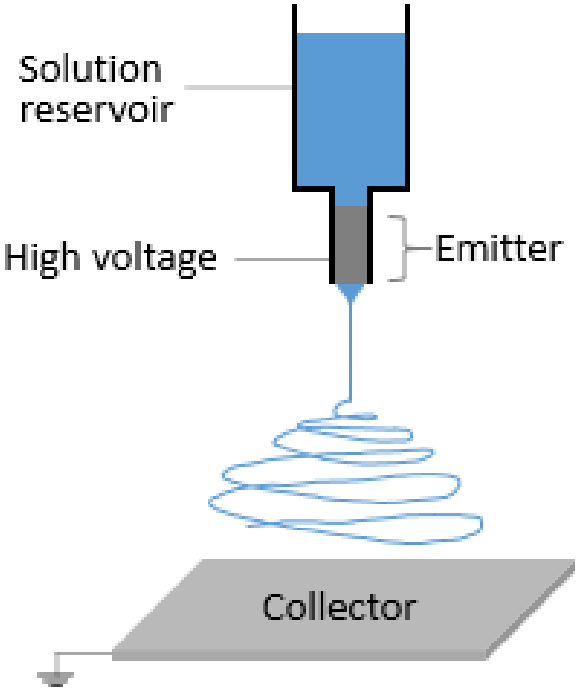

Introduction to Electrospinning cont.

- Using different collectors allows us to create various micro patterns of fibers.
- The diameter of the jet is a function of the surface tension, dielectric constant of the surroundings, flow rate of the liquid, electric current through the jet.

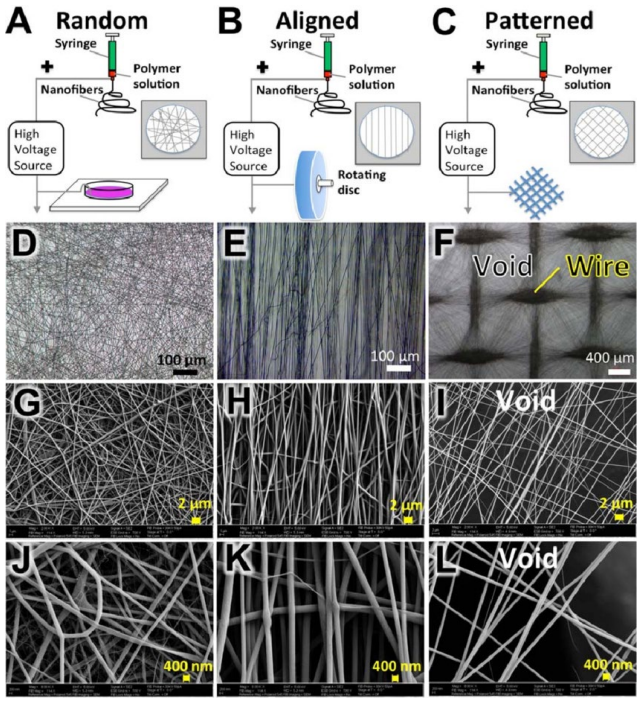

Electrospinning

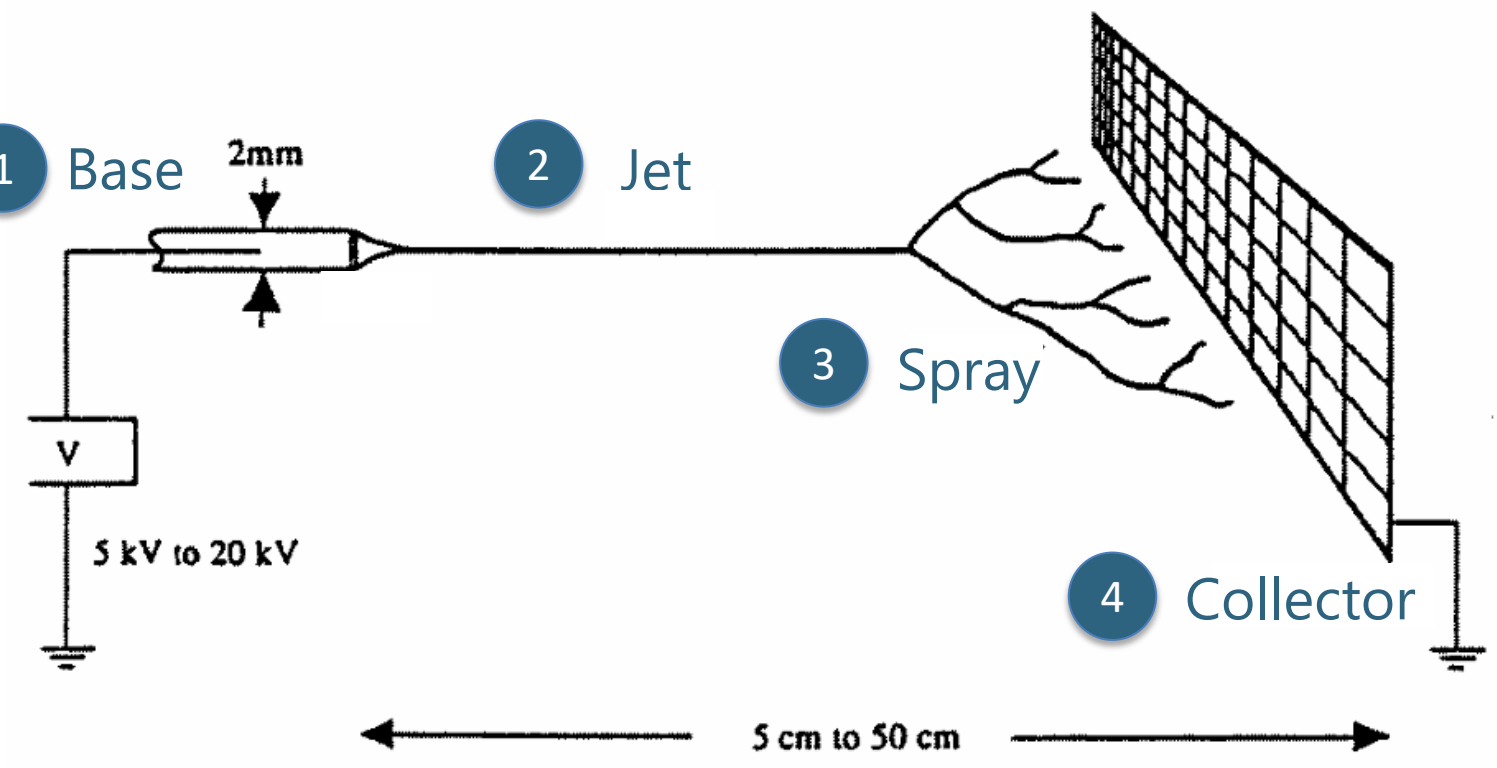

- Electrospun fibers

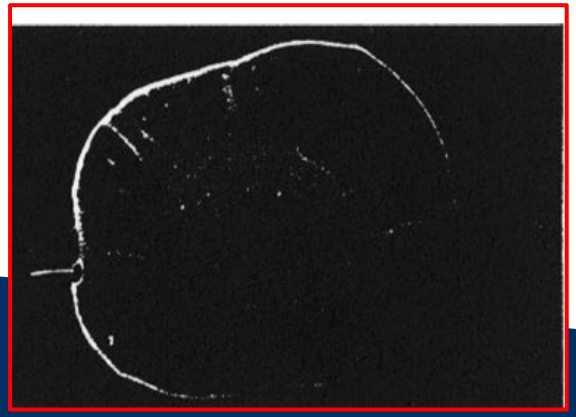

1 Base

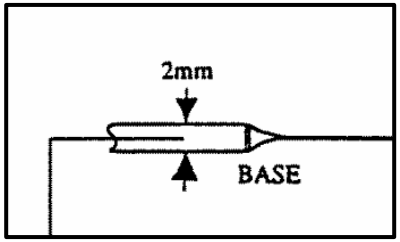

- Tapered Cone

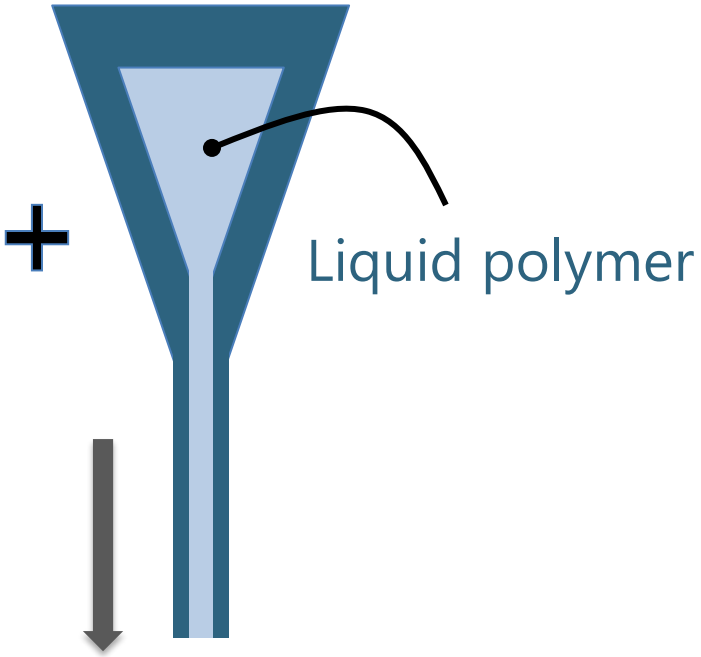

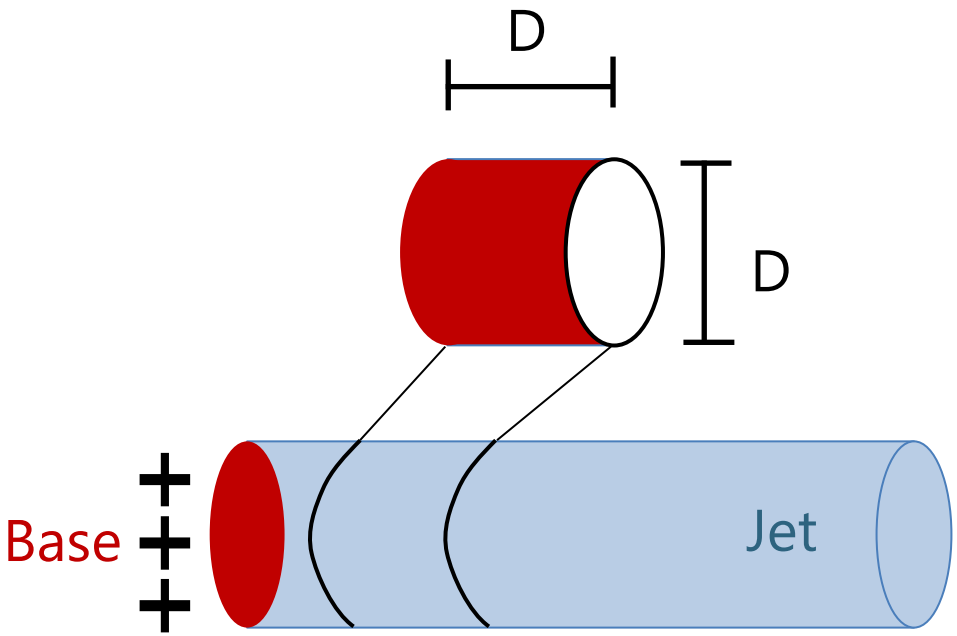

- Charge per unit area conserves

3 The Jet

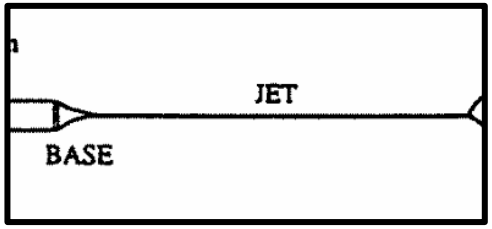

- Electrical charges move⇒ jet velocity ↑
- Jet elongates ⇒ jet velocity ↓

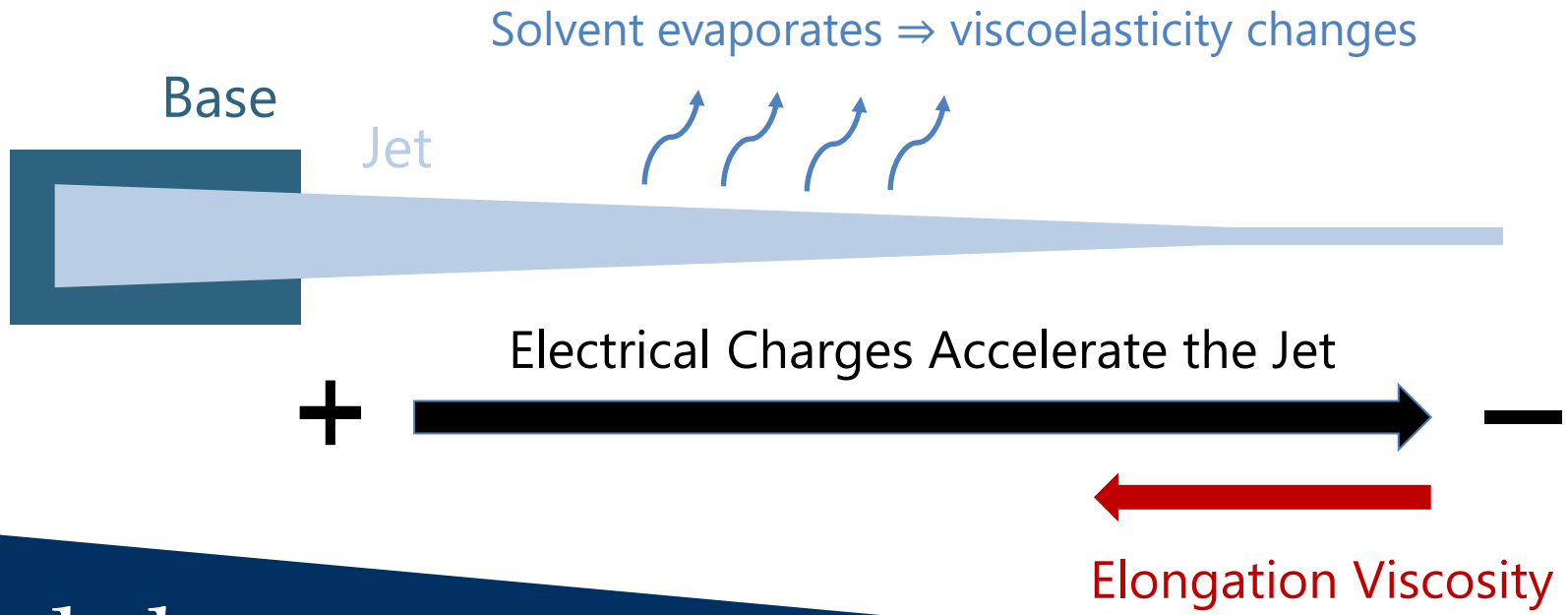

3&4

Splaying & the Collection Region

- F_{radial} from the electrical charges > Jet Cohesive forces

⇒ splay into fibers that repel each other

- Charge migration to the conducting substrate

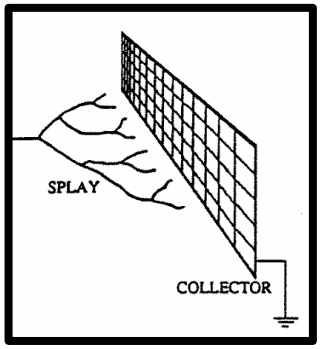

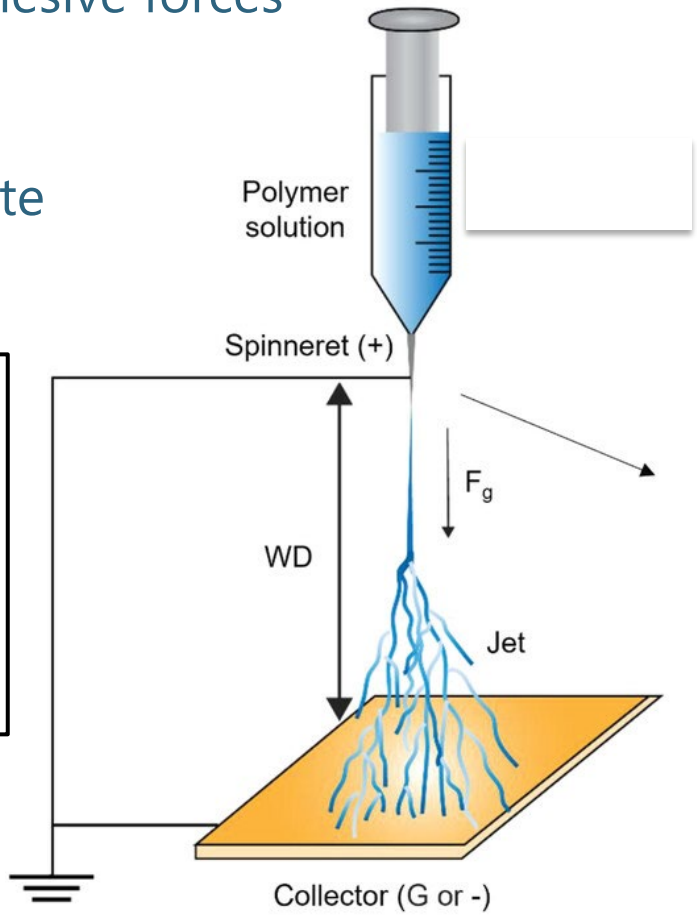

Berkeley
UNIVERSITY OF CALIFORNIA

[Keirouz et al., 2023]

Jet Initiation

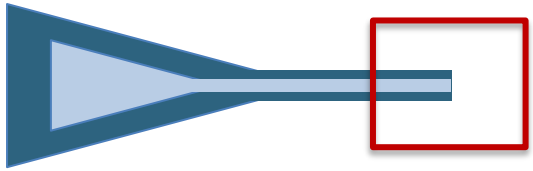

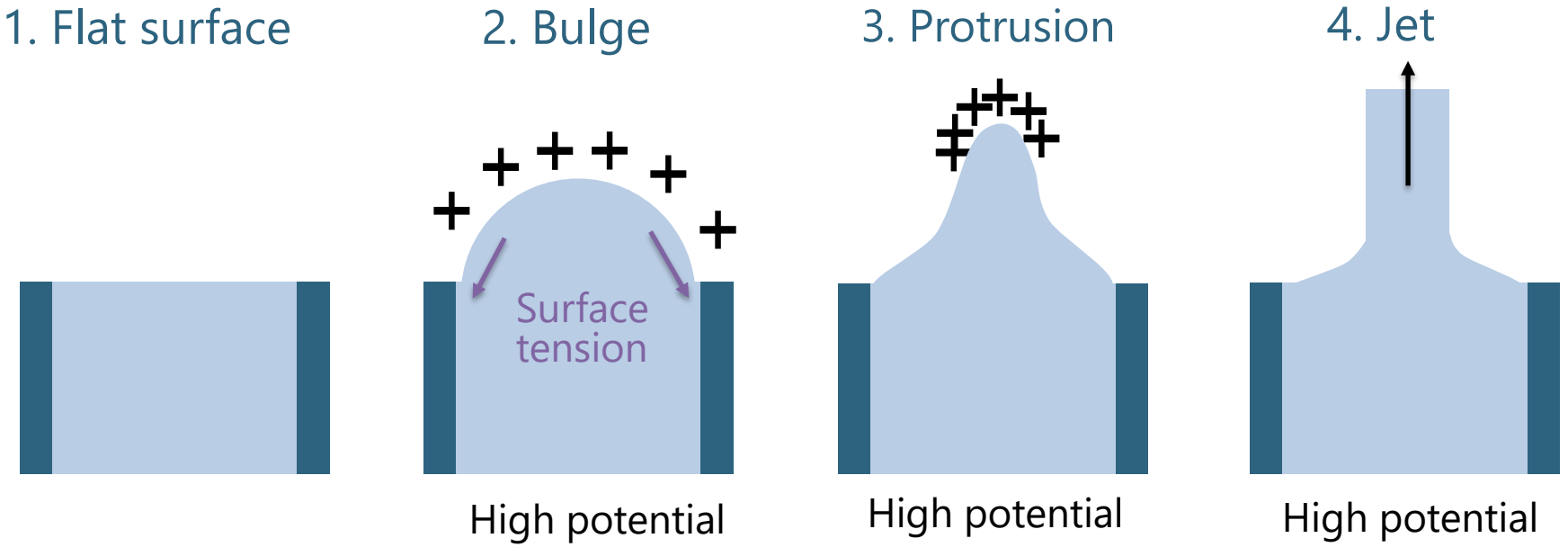

Similar:
Water/oil interface

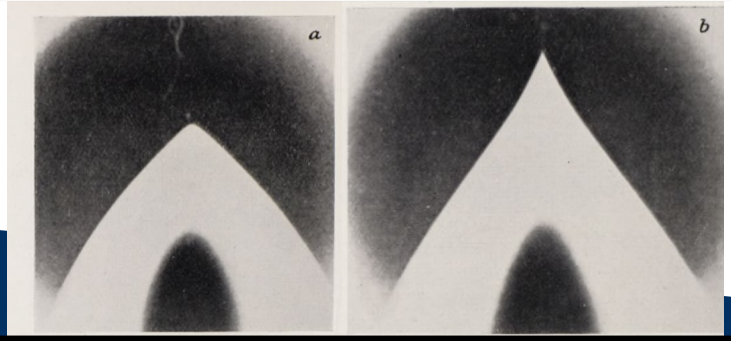

Sir Taylor, 1964

Nanometre diameter fibres of polymer, produced by electrospinning

Part 3 experimental result and application

Peggy Tsao

Berkeley
UNIVERSITY OF CALIFORNIA

Example: electrospinning of polyester fibers-

thin fibers of polyethylene terephthalate

Experimental Setup

- polymer had a molecular weight in the range of 10 000 – 20 000 g / mol
- polymer was dissolved in an equal mixture of dichloromethane and trifluoroacetic acid at a concentration of around 4%
- The fibers were collected on a metal frame about 15 cm and was held about 100 cm from the tip
- The current carried by a typical jet was around 1 μA.

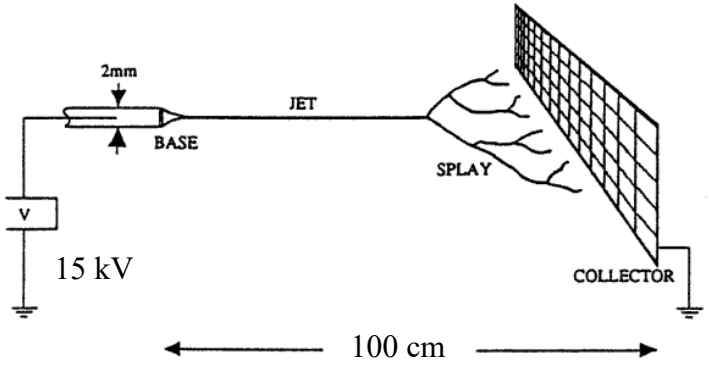

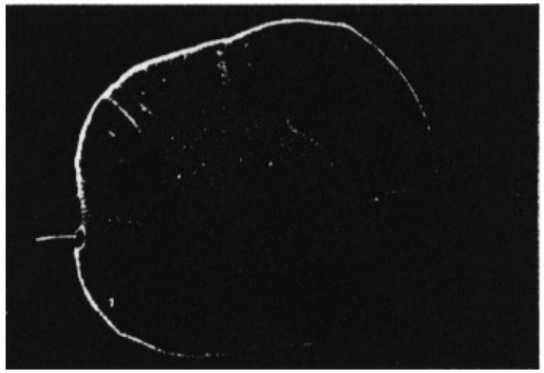

metal frame

Example: electrospinning of polyester fibers-

Result discussion

1. The mechanical attachment of the fibers to each other at crossing points indicate that the fibers were not completely dry when collected.

2. The diameter of fibers are smaller than expected:

- The fibers were cylindrical with a diameters of around 300 nm.
- Based on the setup, the expected value is 2 μm.

Reason:

1. 5 successive splays into two fibers
2. elongation of the fiber by a factor of about 1000.

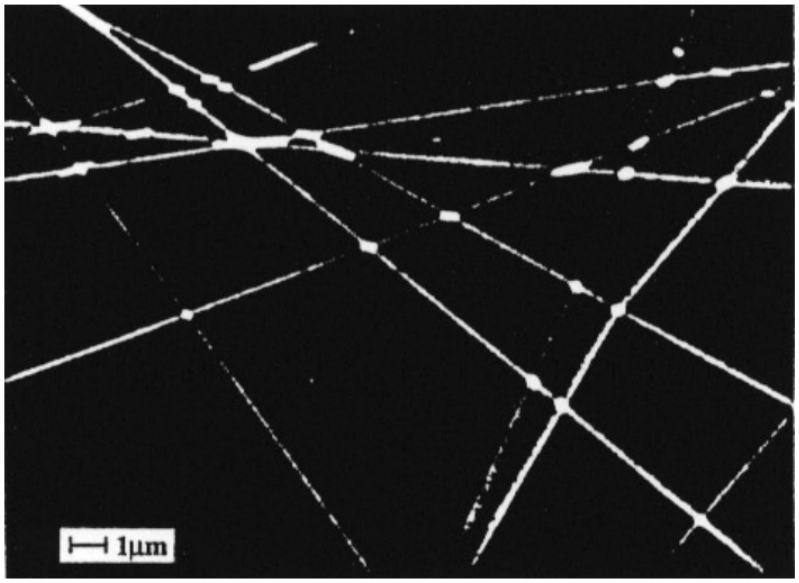

SEM of the fibers

Transmission electron microscopy (TEM)

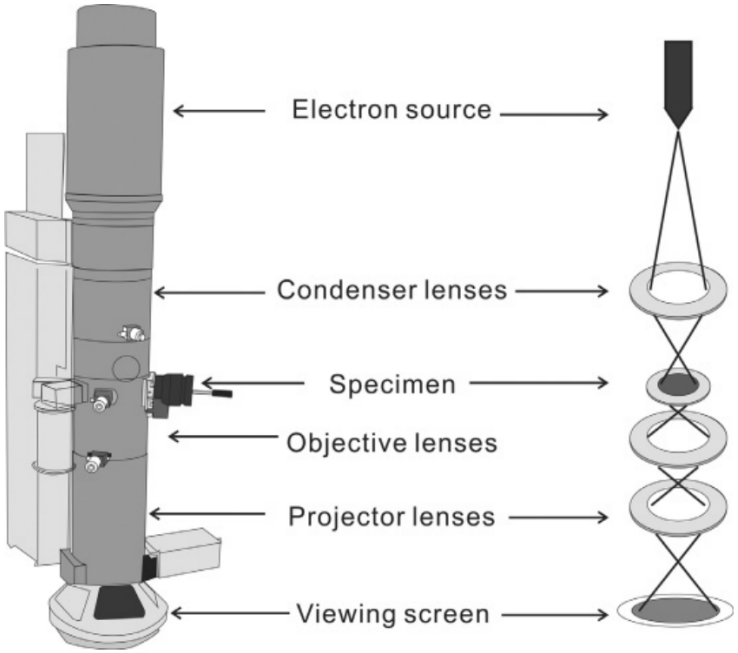

- The polyethylene terephthalate molecules were aligned along the axis of the fiber.

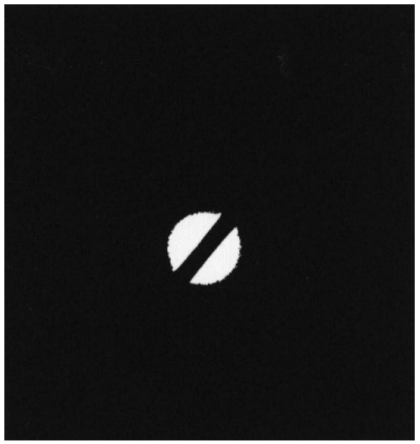

Electron diffraction pattern from an electrospun polyester fibre

Electrospun nanofibers properties and application

Advantages:

Small size

large surface area to volume ratio

high porosity

Application:

Filtration

drug delivery

protective clothing

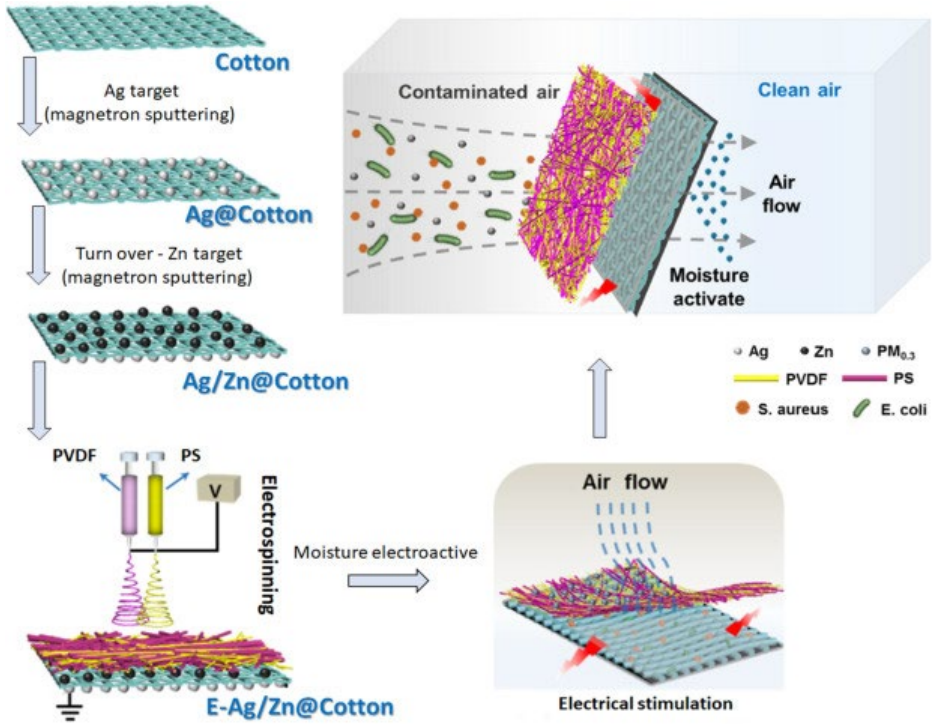

Electrospun nanofibers properties and application

drug delivery

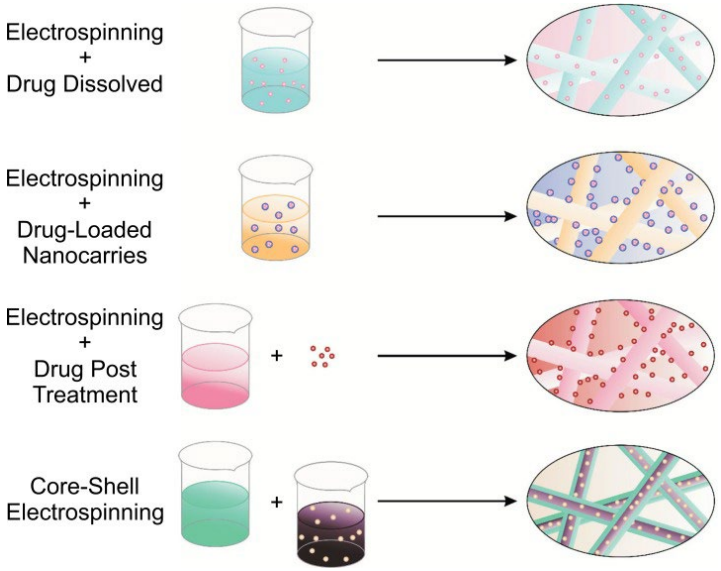

protective clothing

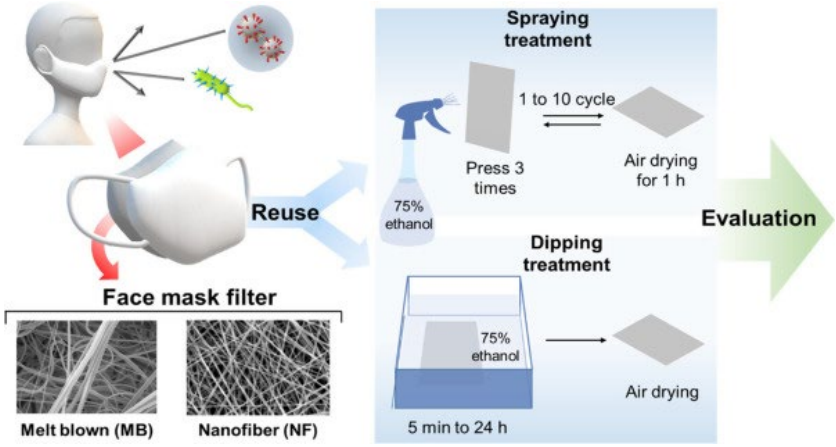

Berkeley
UNIVERSITY OF CALIFORNIA

Enhanced Two-phase Heat Transfer with CNT Heat Sink

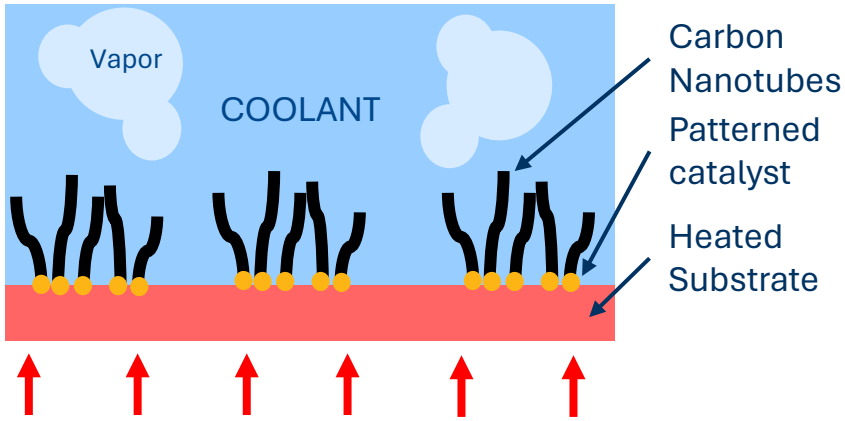

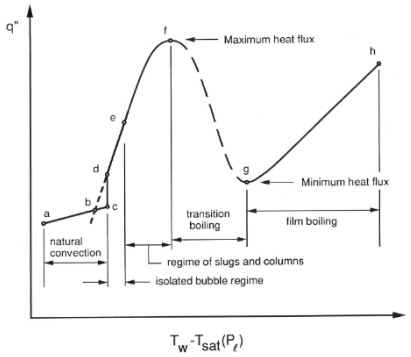

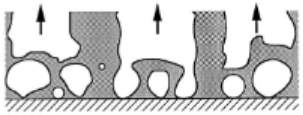

regime of slugs and columns

- Boiling an effective method of absorbing heat for thermal management
- Relevant CNT properties:
  - High thermal conductivity
  - High surface area
  - Wettability (hydrophilic)
- CNT coating has potential to increase heat flux for a given substrate temperature
  - Promoting bubble nucleation
  - Increasing heat transfer area
  - Promoting liquid contact with heated surface

[1] R. Chen, M.-C. Lu, V. Srinivasan, Z. Wang, H. H. Cho, and A. Majumdar, "Nanowires for Enhanced Boiling Heat Transfer," *Nano Lett.*, vol. 9, no. 2, pp. 548–553, Feb. 2009,
[2] G. Stando, S. Han, B. Kumanek, D. Łukowiec, and D. Janas, "Tuning wettability and electrical conductivity of single-walled carbon nanotubes by the modified Hummers method," Sci Rep, vol. 12, no. 1, p. 4358, Mar. 2022.
[3] Van P. Carey, Liquid-Vapor Phase-Change Phenomena : An Introduction to the Thermophysics of Vaporization and Condensation Processes in Heat Transfer Equipment, Third Edition, vol. Third edition. Boca Raton, FL: CRC Press, 2020.

Ben Brown, 03/19/2024

Virus Filtration with CNTs

Michael Celebrado

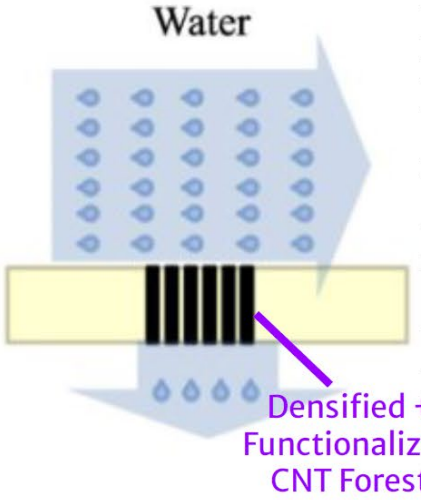

- Ultrafiltration water filters have a pore size of 100 nm
- Viruses (20–400 nm) can bypass these filters
- Can achieve much smaller pore size (< 10 nm) with densified CNT forests[1]
- Viral removal efficiency can be increased with the addition of a phenol group[2]

Process:

1. Grow vertical nanotubes with CVD
2. Mechanical densification by factor Df
   - Compress CNT forest perpendicular to walls
3. Functionalize with phenol group

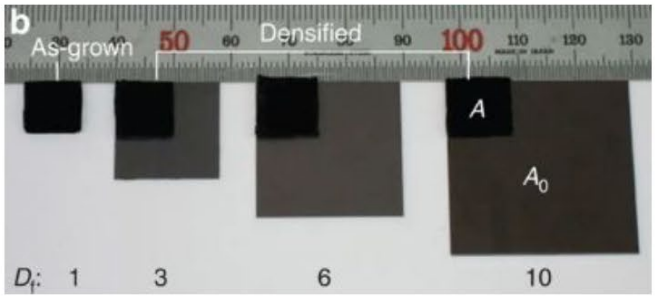

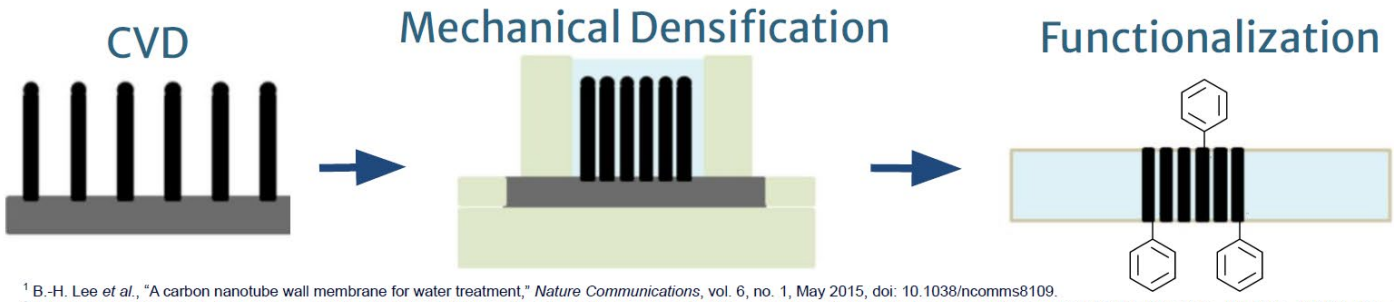

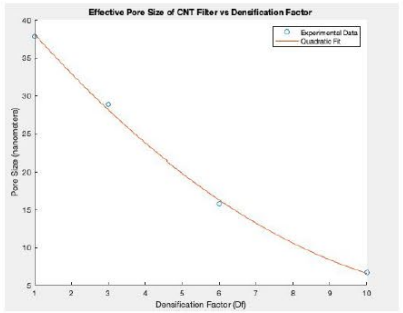

[1] B.-H. Lee *et al.*, "A carbon nanotube wall membrane for water treatment," *Nature Communications*, vol. 6, no. 1, May 2015, doi: 10.1038/ncomms8109.
[2] I. Gupta, S. Azizighannad, E. T. Farinas, and S. Mitra, "Antiviral properties of select carbon nanostructures and their functionalized analogs," *Materials Today Communications*, vol. 29, p. 102743, Dec. 2021, doi: 10.1016/j.mtcomm.2021.102743.

MOF-Enhanced Nanowire Gas sensor

Goal: Find a MOF that functionally selective for specific gases that would enhance Nanowire Gas Sensor sensitivity.

Proposal:

- Make use of specific most that have preference to certain gases to increase the sensitivity of nanowires
- In essences increase the surface area and attractiveness of the gas to the nanowire
- Match the pore size to the molecule which is desired to be detected.
- Expand these system to more than H_2 eg. methane, benzene, toluene
- Make use of other nanowires that would optimize the sensor

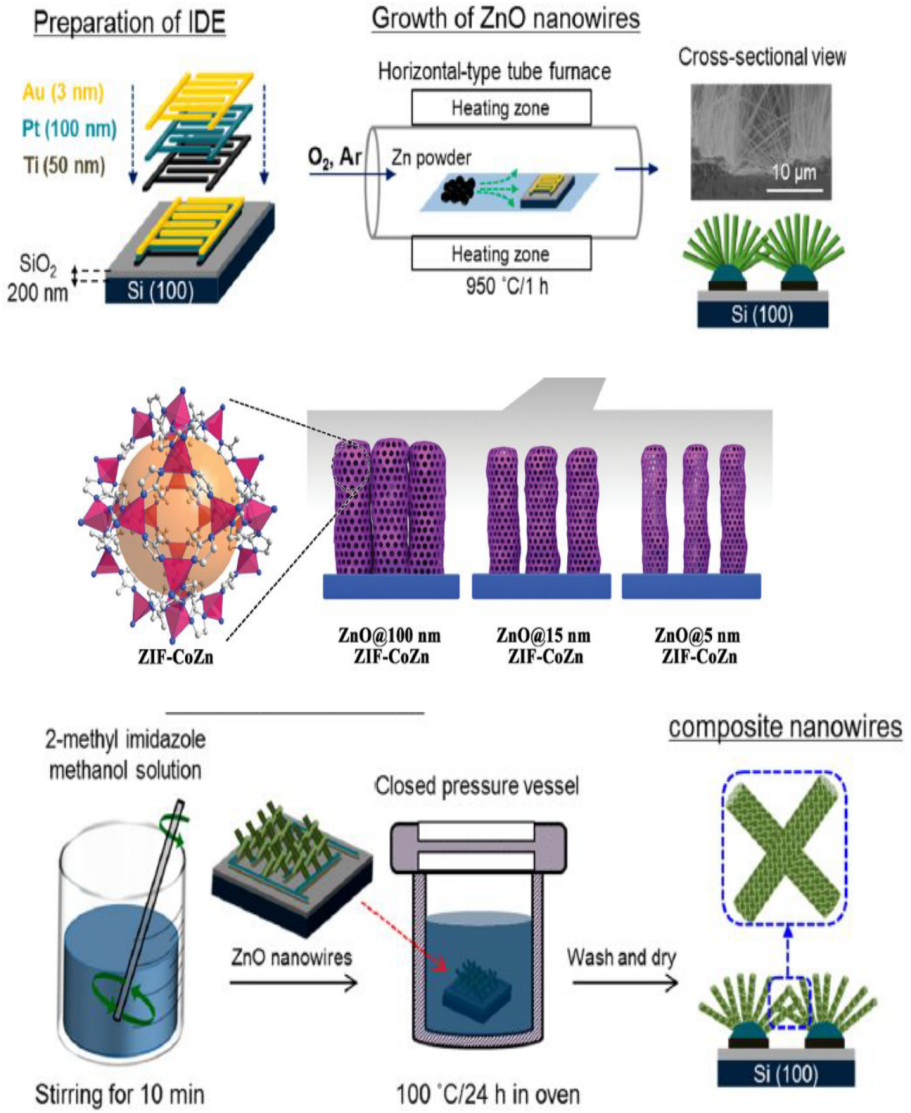

1. Martin Drobek, Jae-Hun Kim, Mikhael Bechelany, Cyril Vallicari, Anne Julbe, and Sang Sub Kim ACS Applied Materials & Interfaces **2016** *8* (13), 8323-8328
2. Yao, M.-S., Tang, W.-X., Wang, et al, G. MOF Thin Film-Coated Metal Oxide Nanowire Array: Significantly Improved Chemiresistor Sensor Performance. Adv. Mater., **2016** 28: 5229-5234

Carbon Nanotubes for Space Elevator Tether

Current Tether Challenges:

- 100,000km long
- Tensile strength need is 50 Gpa (steel is 5 Gpa)
- Volume of Cable (approx 1 meter x 15 microns)

CNT Proposal:

- Tensile strength is approx 150 Gpa
- Density ~1300 kg/m^3
- High strength to volume ratio

Producing Long CNT's is difficult. In FDM printing we can add chopped fiber to reinforce parts. Add short CNT's throughout continuous steel cable. CNT melting temp: 3550 °C and Steel melting temp: 1370° C

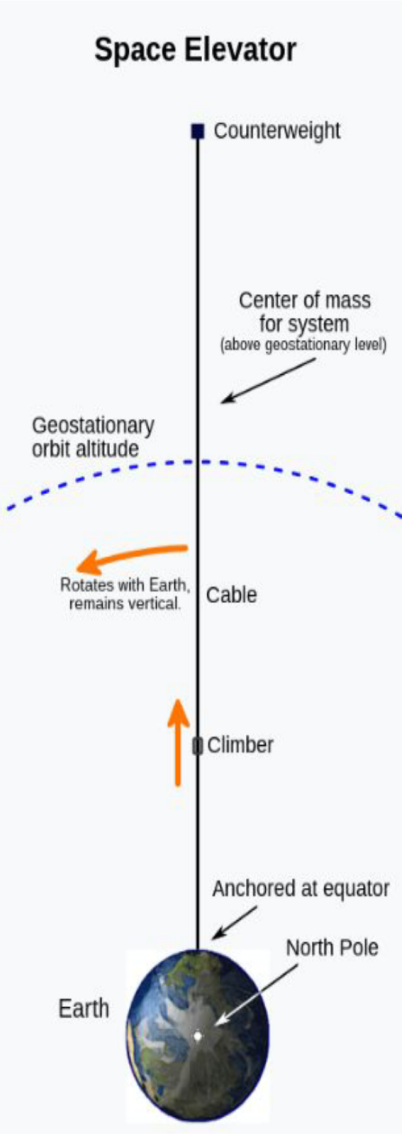

References:
Nanotechnology Application: Space Elevator, MRSEC Education Group
Space Elevator Tether Materials: The Crux of the Matter, ISEC
Graphene Progress and It's Promising Future for Space Elevators, GEIC
Space Elevator: A Futuristic Application of Carbon Nanotubes, Nanografi
Making Carbon Nanotubes into Long Fibers, Katherine Bourzac
UC Researchers Shatter World Records with Length of Carbon Nanotube Arrays, University of Cincinnati

Luke Goldade

Carbon Nanotubes in Recreation of Damascus Steel

Damascus Steel Information

- Lost ancient technique used for Fine Blades
- Remarkable Mechanical Properties
  - Sharpest Blade ever made before introduction of modern material and industrial process
  - High strength & resilience
- Made from "Wootz Steel" which contains 1-2 wt% amount of carbon, which is normally brittle due to the presence of cementite

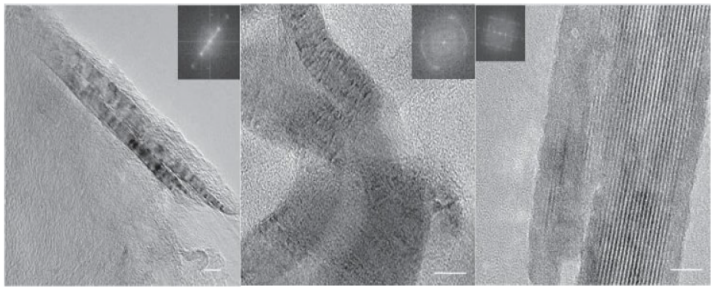

High-resolution TEM images of carbon nanotubes in a genuine Damascus sabre after dissolution in HCI (Reibold 2006).

CNT Proposal for Manufacturing of Steel Blades

- Introduce modern manufacturing process of CNTs during blade-treatment procedure, such as patterned catalyst
- Cyclic forging makes catalyst to mixed up inside the alloy and cause CNT growth
- Formation of MWCNTs in the nanostructure of the steel alloy could recreate the properties of Damascus Steel

Ke Hu

Reibold, M., Paufler, P., Levin, A. et al. Carbon nanotubes in an ancient Damascus sabre. Nature 444, 286 (2006)
Verhoeven, J. D., Pendray, A. H. & Dauksch, W. JOM 56, 17–20 (2004).

Detecting Methyl Iso Cyanide with B(OH)-Doped CNTs

Possibility of hydrogen bond forming between B(OH) and MIC molecule from its O or N head, gave us an idea to explore adsorption of MIC molecule on B(OH)-Doped CNTs

Navin Vijey Raj Jeyaselvan (2024) MEng Mechanical Engineering

Assumptions:

- B(OH) can be attached as a functional group to the CNTs.
- B(OH) group remains attached to the CNTs during their assembly and integration.

Formation of CNT's With Borinic Functional Group

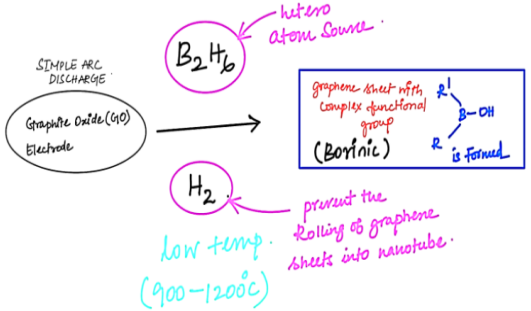

Reference : Agnoli, S. and Favaro, M., 2016. Doping graphene with boron: a review of synthesis methods, physicochemical characterization, and emerging applications. Journal of Materials Chemistry A, 4(16), pp.5002–5025. DOI: 10.1039/c5ta10599d.

From the above Process the Hydrogen can be removed to allow the formation of the CNTs With the Boronic Functional group (Approx 3 to 4 % Doping)

CNT's Assembly and Integration

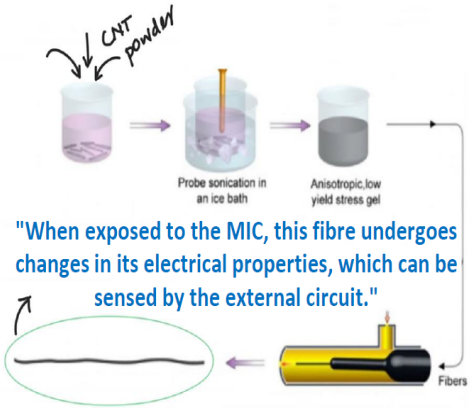

Reference : Venkataraman, A., Amadi, E. V., Chen, Y., & Papadopoulos, C. (2019). Carbon Nanotube Assembly and Integration for Applications. Nanoscale Research Letters, 14(1), 220. https://doi.org/10.1186/s11671-019-3046-3

Positive H atom is located between two most negative O atoms and therefore, strong interaction between MIC molecule and B(OH)- graphene is formed.

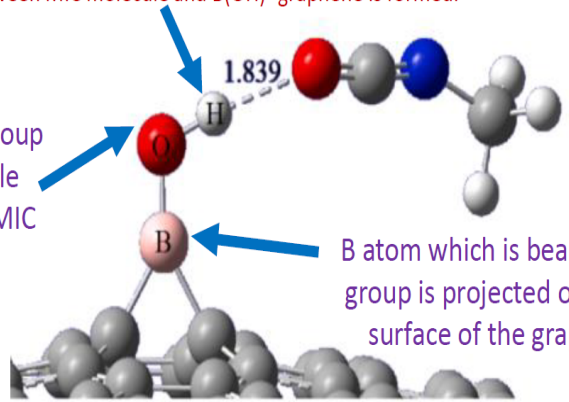

Configuration	E_{HOMO}	E_{LUMO}	E_g
B(OH)-doped graphene	−3.97	−1.81	2.16
MIC/B-OH-doped graphene	−3.11	−0.91	2.20

The Fermi level is largely shifted to higher energy after adsorption of MIC molecule.

Why B (OH) Group ?

- Boron is less electronegative than carbon and induces p-type conductivity in CNTs.
- The doping of boron can improve chemical and electrochemical activity of the CNTs.

Reference : Rouhani, Morteza. "Computational Evaluation of B(OH)-Doped Graphene Efficiency for Detecting Methyl Isocyanate (MIC)." *Inorganic Chemistry Communications* 127 (2021): 108552. ISSN 1387-7003. https://doi.org/10.1016/j.inoche.2021.108552.

NanoFilm Airflow Sensor

Michael Jia

- Purpose:
  - Minimize device size for measuring mass airflow for aeronautics and automotive airfoil surface optimization.
    - Important to be able to accurately measure empirically wind and pressure data from aerofoils to compare with simulations to develop more accurate methodologies of simulation of real world conditions.
  - Current applications to measure wind speed for vehicles and airplanes is pitot static tube mounted on leading edge which are generally large and require a pressure chamber as well as a pressure transducer in order to work.
- Method/Theory:
  - Grow forest of CNT on electrical circuitry wires on a film like substrate and sandwiched with another film like substrate on top using a CVD methodology with catalyst seeded on top of film like substrate.
  - Attach film substrate and CNT forest sandwich with adhesive backing to a surface in question to measure resistance change as CNTs that join one film to another are disconnected due to the force and speed of the air stream increasing resistance.
- Measurement/Results:
  - Apply a known voltage potential across film substrate and CNT forest sandwich.
  - Characterization of no flow resistance of sandwich to form baseline resistance value.
  - Apply sensor on surface and measure current decrease as resistance increases as fewer CNTs join film like substrates in sandwich creating fewer parallel paths for current to flow.
  - Measurements of current decrease with constant voltage supplied can correlated with air flow speed in air stream to result in almost invisible skin like sensors on aerofoil surfaces

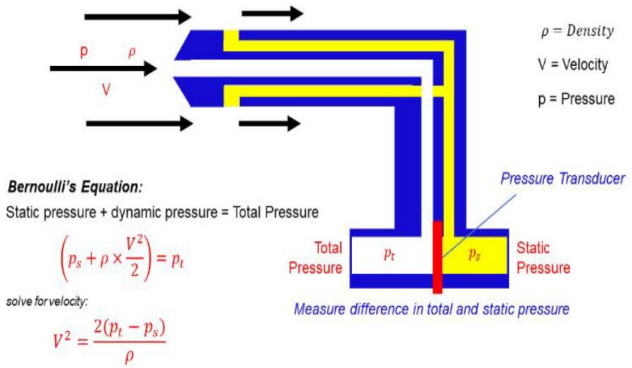

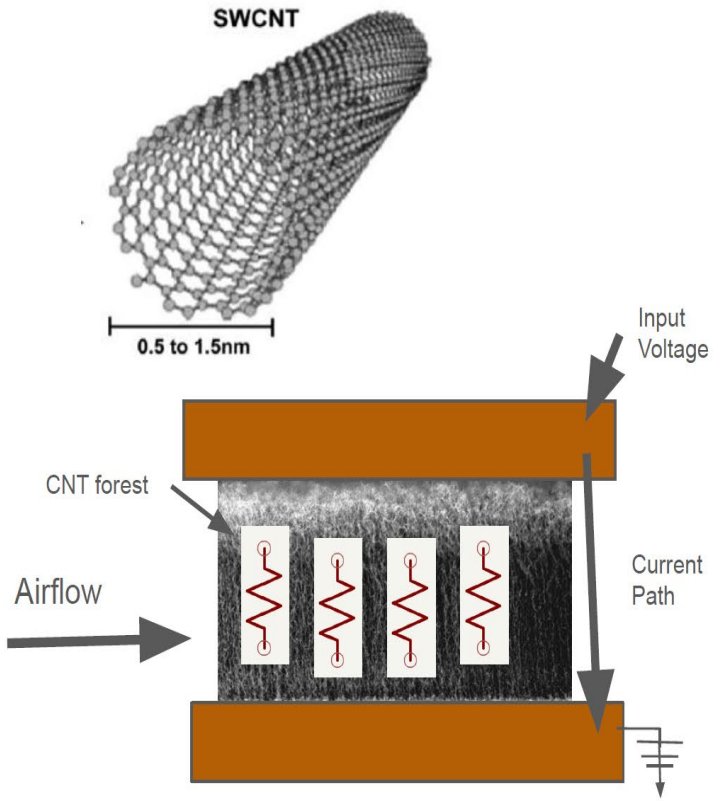

Synergistic Use of TiO2 and Ag Nanowires for Advanced Water Filtration to Remove Malaria-Carrying Plasmodium Parasites

By Evan Kaplan and Anugreh Kaul

- Various nanowire structures (commonly hydroxyapatite nanowires (HAPNWs) and cellulose fibers (CFs)) have been used to filter water of organic pollutants due to their high surface area to volume ratio and variable densities.
- We aim to use a combination of of TiO2 and Ag nanowires to uniquely target malaria-carrying parasites which range in diameter from 1-20 microns.
  - TiO2 nanowires are photocatalysts that generate reactive oxygen species (ROS). Upon absorbing photons during UV light irradiation, TIO2 undergoes electron-hole pair generation, leading to the production of reactive species such as hydroxyl radicals which can degrade microbial pathogens.
  - Ag nanowires release Ag+ ions when combined with water, disrupting microbial cell membranes and enzyme activity, leading to cell death.
  - Using template assisted growth for Ag nanowires and hydrothermal synthesis for TiO2 sheets, we can employ electrospinning to deposit silver nanowires into the TiO2 structure. Finally post treatment such as annealing can purify the composite material which was be characterized using techniques such as SEM/TEM.

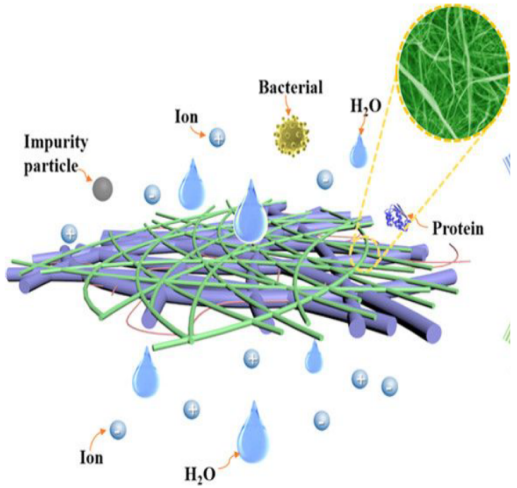

Qiang-Qiang Zhang, Ying-Jie Zhu, Jin Wu, Yue-Ting Shao, An-Yong Cai, and Li-Ying Dong ACS Applied Materials & Interfaces 2019 11 (4), 4288-4301
DOI: 10.1021/acsami.8b20703

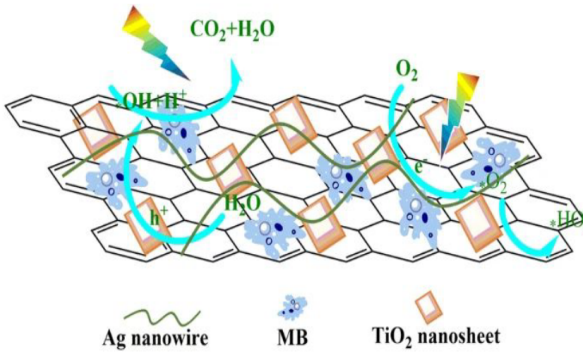

Liu, C., Lin, Y., Dong, Y. *et al*. Fabrication and investigation on Ag nanowires/TiO_2 nanosheets/graphene hybrid nanocomposite and its water treatment performance. *Adv Compos Hybrid Mater* **3**, 402–414 (2020). https://doi.org/10.1007/s42114-020-00164-2

Tunable VO_2 Nanowire Thermoelectric Device

Tune electrical conductivity

$$ZT = \frac{S^2\sigma}{k}\mathrm{T}$$

VO_2 changes phase at T_c and becomes metallic

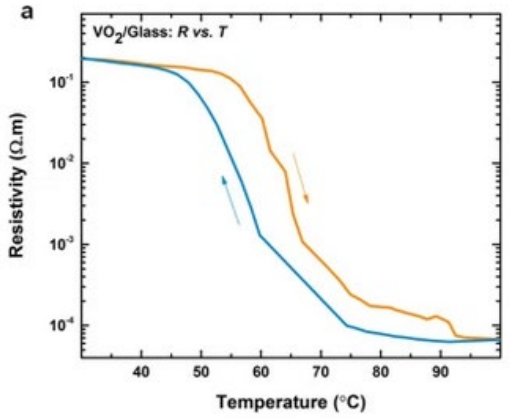

- Thermoelectric effect suppressed below T_c
- T_c changes with applied stress

Main application:

- Autoregulated heat dissipation in electronics (~80C)

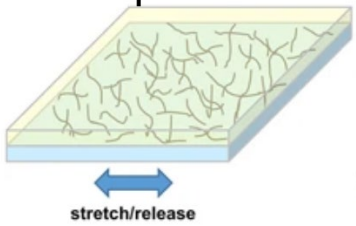

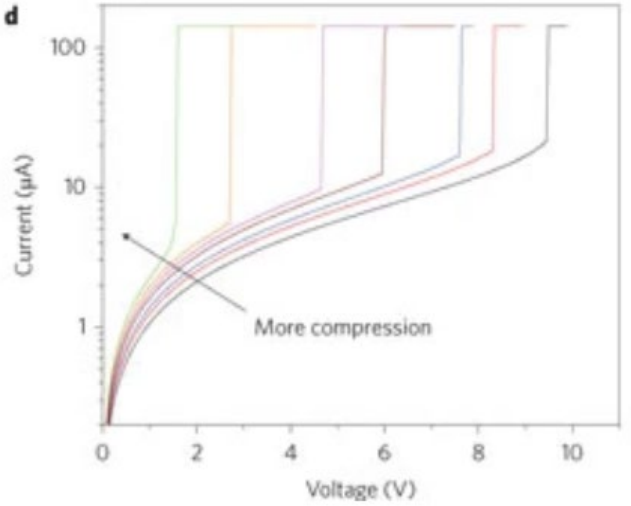

Insulator–metal transition in substrate-independent VO2 thin film for phase-change devices, Mohammad Taha et al.
Strain engineering and one-dimensional organization of metal–insulator domains in single-crystal vanadium dioxide beams, J. Cao et al.